Developing a Geologically-Based V_{S30} Site-Conditions Model for Portugal: Methodology and Assessment of the Performance of Proxies

Susana P. Vilanova[1] and João Narciso, João P. Carvalho, Isabel Lopes, Mário Quinta-Ferreira, Carlos C. Pinto, Rui Moura, José Borges, Eliza S. Nemser

[1]Corresponding Author; Centro de Recursos Naturais e Ambiente, Instituto Superior Tcnico, Universidade de Lisboa, Av. Rovisco Pais 1, 1049-001, Lisbon, Portugal; susana.vilanova@tecnico.ulisboa.pt;

The electronic supplement to this paper contains the V_{S30} database flat-file developed and used in the context of the paper.

November 8, 2017

Abstract

The inclusion of site-specific conditions is essential to adequately represent the seismic hazard and the seismic risk for a region. We acquired, gathered and organized a near surface shear-wave velocity database for Portugal, and applied a three-step methodological approach for developing a V_{S30} site-conditions map using extrapolation based on surface geology. The methodology includes: 1) defining a preliminary set of geologically defined units; 2) calculating the probability distribution of $\log V_{S30}$ for each unit; and 3) merging the units according to the results of statistical tests. The final model comprises three geologically defined units characterized by $\log V_{S30}$ distributions that are statistically significantly different from each other: F1 - Igneous, metamorphic and old sedimentary rocks; F2 - Neogene and Pleistocene formations; and F3 - Holocene formations. The site conditions for F3 unit may be further refined using correlations with topographic slope based on the SRTM3 dataset. We analysed the performance site-conditions models based on correlations with exogenous data (topographic slope and surface geology analogues). The results show that the residual distributions between $\log V_{S30}$ values measured and estimated from those proxies are strongly biased for some geological units, emphasizing the need for acquiring regional V_S data.

Introduction

Earthquake ground motion maps such as seismic hazard maps or instrumental intensity maps provide critical information for a variety of societal applications. They support decision-making processes that include the development of regulatory legislation, the estimation of insurance rates, land-use planning and emergency planning. Since local site conditions strongly affect the characteristics of ground motion, estimating first-order site-conditions at the regional scale is essential for improving the information delivered by such maps.

The importance of the near-surface shear-wave velocity (V_S) structure on ground motion amplification is supported by both theoretical considerations (e.g., Aki and Richards, 1980; Stein and Wysession, 2009) and observational studies (e.g., Joyner *et al.*, 1981; Borcherdt, 1994). Within unbounded and homogeneous media V_S is proportional to the square root of the quotient between the shear modulus and the density of the medium. Both the shear modulus and the density tend to increase with depth and the overall tendency of V_S is to decrease as the waves propagate from depth towards the surface. This reduction of V_S has important implications for the conservation of elastic energy. For vertically propagating SH waves in an elastic medium the energy flux is given by the product of density and V_S (seismic impedance) and the particle velocity squared (e.g., Aki and Richards, 1980). Because the conservation of energy requires the flux to remain constant, the decrease of impedance needs to be compensated by the increase in particle velocity and therefore amplitude of the seismic wave. This effect is however partially counteracted by that of anelastic attenuation, which tends to be greater on soft soils (e.g., Reiter, 1990; Kramer, 1996).

The modification of ground motion by site-conditions, usually referred to as site-effects, includes local ground response, basin effects, and topographic effects (e.g., Stewart *et al.*, 2001; Kamai *et al.*, 2016). Local ground response represents the effects of the variation of the physical properties of the near-surface materials on nearly-vertically propagating SH waves. In local ground response abrupt changes in medium impedance at depth result in large amplification at specific frequency ranges of ground motion (resonance). Both basin and topographic effects refer to the influence of 2-D or 3-D geometric configurations on the propagation of seismic waves, and its importance, which can be large, is usually restricted to specific locations. Although the detailed study of site-effects is essential for site-specific studies, regional assessments must necessarily rely on simplified approaches.

Joyner *et al.* (1981) proposed the use of a quantitative V_S-based parameter for a simplified representation of site conditions the V_S corresponding to the depth associated with one quarter-wavelength at the period of interest. Due to the economical constraints associated with obtaining data at the required depths this measure has been superseded by the use of the time averaged V_S to 30 m depth, given by

$$V_{S30} = \frac{30}{\sum t_i} \tag{1}$$

where t_i is the traveltime of the S wave within each layer up to the depth of 30 m.

Borcherdt (1994), based on previous empirical work, recommended the use of V_{S30} for classifying sites for building codes and the parameter is included in both in the National Earthquake Hazard Reduction Program (NEHRP) seismic design provisions (e.g., BSSC, 2004) and in the Eurocode 8 (CEN, 2004).

Because V_{S30} is strongly correlated with deeper velocity structures (Boore, 2004; Boore *et al.*, 2011) it has been shown to describe site-effects at ground motion frequencies corresponding to wavelengths much longer than 30 m (Stewart *et al.*, 2014).

V_{S30} has increasingly become the reference parameter for classifying site conditions in several applications. It is currently used for characterizing site-conditions in ground motion prediction equations, and for modeling ground motion amplification in both seismic hazard maps and instrumental intensity maps. It has long been known that V_{S30} present several limitations as a site-conditions parameter (e.g. Castellaro *et al.*, 2008). Additional parameters, such as the natural frequency of the site, are being investigated for improving the regional site characterization in a variety of applications (e.g. Cadet *et al.*, 2010; Motazedian *et al.*, 2011; Hassani and Atkinson, 2016).

Developing V_{S30} Site-Conditions Maps

Estimating spatially-continuous variables from discrete datasets requires either the correlation with spatially extensive datasets or the application of extrapolation or interpolation techniques.

Surface geology-derived classification schemes have been used to produce regional V_S site conditions maps based on rock type and/or geological age (e.g., Tinsley and Fumal, 1985; Park and Elrick, 1998; Wills and Silva, 1998). The correlation between V_S and geologic units relies on the fact that V_S depends on physical properties of the materials such as density, porosity, cementation, and fracture spacing.

Wills and Silva (1998) correlated V_{S30} data with geologic units in California and extrapolated based on surface geology in order to obtain a statewide map of V_{S30}. That approach has been further refined by using depositional environment and geographic criteria as additional constraints (Wills and Clahan, 2006; Wills *et al.*, 2000). Similar approaches have been also used for the state of Utah (e.g., Ashland and McDonald, 2003; McDonald and Ashland, 2008).

Park and Elrick (1998) developed a geologically-based (V_{S30}) map for the southern California region. Their approach differs from that of Wills and Silva (1998) in that their goal was to achieve the simplest model supported by the dataset. To attain that objective they used statistical tests (the t-test and the Komolgorov-Smirnov test) to justify the subdivision of an initial set of geological units, if statistically significant.

The most extensively used V_{S30} extrapolation method is however that based on topographic slope. The approach, which has been introduced by Wald and Allen (2007), relies on the correlation of V_{S30} measurements and the topographic slope for both regions of active tectonics and stable tectonics. Although there is no explicit physical relationship connecting V_{S30} and topographic slope, it is expected that the later will relate to different geomorphologic environments and lithology in a broad sense, since more competent high-velocity materials can maintain a steep-slope, whereas fine basin sediments will be deposited in nearly-flat basins. The main advantage of the method is that since topographic data are globally available, a V_{S30} model can be derived for any region. One of the limitations of the model is that it is not expected to be effective in regions of flat-lying rocks.

When dense V_S datasets are available and the values are spatially correlated geostatistical interpolation tools can be used to develop spatially-continuous V_{S30} models. Thompson *et al.* (2007) employed such an approach for mapping V_{S10} in the San Francisco Bay Area, finding spatial horizontal correlations on the order of 4 km.

Thompson *et al.* (2014) presented a framework that combines surface geology maps with topographic data for developing V_{S30} maps. Their approach is based on identifying trends between surface-geology derived V_{S30} residuals and topographic slope. The results show that both Quaternary alluvium and Pleistocene sedimentary units exhibit trends with topographic gradient. They applied a kriging-with-a-trend technique to obtain a final V_{S30} map for California.

The terrain-based classification is an automatic procedure developed by Iwahashi and Pike (2007) and relies on the development of a set of geomorphic categories based on gradient, convexity and surface texture, using an automatic procedure. This methodology has been applied to characterize V_{S30} in California with promising results (Yong *et al.*, 2012).

Due to the scarceness of shear-wave velocity data in most regions, models developed for data-rich regions have been employed to estimate site conditions elsewhere. In particular, the topographic slope method has become the standard way for incorporating site effects into regional studies worldwide given the convenience provided by the global V_{S30} server (Allen and Wald (2007); see Data and Resources).

Lemoine *et al.* (2012) evaluated the performance of the topographic slope method for stable and active regions of Europe using the V_{S30} dataset compiled in the context of project SHARE (Seismic Hazard Harmonization in Europe). The results show that while the method provided better estimates than pure randomness for active regions that was not the case for stable continental regions. Lemoine *et al.* (2012), however, acknowledged the fact that their analysis for stable continental was based on a very limited dataset.

Stewart *et al.* (2014) compiled and analyzed a large V_S dataset for Greece. They propose a framework for estimating V_{S30} for sites in Greece based on geology and slope. They recommend both the geology-slope approach and the terrain approach of Yong *et al.* (2012) over the slope approach of Wald and Allen (2007). They nevertheless acknowledge that the latter is probably the only available approach for many regions of the world.

Project SCENE, funded by the Portuguese Foundation for Science and Technology (FCT), aimed at gathering and acquiring shear-wave velocity profiles in diverse lithological and geological formations in Portugal, in order to 1) characterize sites where strong-motion stations are deployed and 2) develop a regional site conditions map to be used in seismic hazard maps.

In this paper we focus on the methodological approach used for developing a statistically robust site-conditions map for Portugal. The database includes 160 V_S profiles and is the largest published for stable continental regions, making it particularly suited to test the applicability of proxies based on exogenous V_S empirical correlation.

Brief Tectonic and Geological Setting of the Study Region

The study area, Portugal, is located in the western region of the Iberian Peninsula, within the Eurasian tectonic plate (Figure 1a). It is defined as a stable continental region according to the geological criteria proposed by Johnston (1989), and displays moderate seismicity rates (e.g., Custódio *et al.*, 1996). The seismic record for Portugal includes several intraplate earthquakes with magnitude estimates in the $\mathbf{M}6.0 - \mathbf{M}7.3$ range, both historical (Vilanova and Fonseca, 2007; Stucchi *et al.*, 2013) and pre-historical (Rockwell *et al.*, 2009; Canora *et al.*, 2015). Western Iberia is also affected to some extent by the large to great interplate earthquakes nucleating in the Azores-Gibraltar plate boundary, such as the $\mathrm{M_S}7.8$

1969 earthquake (Fukao, 1973) and the **M**8.5−**M**8.7 1755 Lisbon earthquake (e.g., Johnston, 1996; Vilanova *et al.*, 2003; Martínez Solares and López Arroyo, 2004; Fonseca, 2005).

Portugal displays in general moderate hazard levels ($0.1\,\mathrm{g} \leq \mathrm{PGA} \leq 0.25\,\mathrm{g}$ for 10% exceedance probability in 50 years) according to the 2013 European Seismic Hazard Map (Woessner *et al.*, 2015). This result is consistent with the previous regional study by Vilanova and Fonseca (2007).

The basement of the Iberian Peninsula, known as the Hesperic Massif, or Iberian Massif, is composed of igneous and metamorphic rocks of Paleozoic and Precambian ages, which have been accreted together during the Paleozoic. The Hesperic massif represents the largest continuous exposure of the Variscan Orogen in Europe. Above this cratonic block several basins developed in both the western and southern margins as a consequence of the rifting episodes that, during the Mesozoic, led to the opening of the Atlantic Ocean and the Tethys Ocean. These basins have been further deformed and inverted during subsequent compressive tectonics in the Eocene (Pyrenean Orogeny) and Miocene (Africa-Eurasia collision). Further details on the geology and geological evolution of the region can be found, for instance, in Ribeiro *et al.* (1979), Pinheiro *et al.* (1996) and references therein.

Data and Methods

Both invasive and non-invasive methods can be employed to characterize the near-surface structure of the shear-wave velocity. Determining the shear-wave velocity using invasive methods involves directly measuring the wave travel-time to a range of depths. Non-invasive methods involve the acquisition of waves at the surface and require the use of an inversion algorithm and/or forward modeling to resolve the structure at depth.

Although invasive methods are well known and highly reliable, the non-invasive approaches are significantly less costly. The latter also have the advantage of providing a more spatially extensive sample of the subsurface. Comparisons between invasive and non-invasive data at same sites show that, in general, compatible velocity structures or V_{S30} values are obtained (e.g., Xia *et al.*, 2002; Williams *et al.*, 2003; Scott *et al.*, 2006; Boore and Asten, 2008). Moss (2008) evaluated the intramethod uncertainty in measuring V_{S30} from different techniques both invasive and non-invasive reporting coefficients of variation on the order of 1%-3% for invasive techniques and 5%-6% for non-invasive techniques.

Seismic Refraction

We used seismic refraction as the main tool for characterizing the shear-wave subsurface structure at the selected locations. The seismic refraction is a widely known and applied method in geophysics. It uses active seismic sources at the surface and involves measuring the travel times of the seismic waves as they travel from the source towards a set of aligned receivers. Assuming that wave velocity increases with depth, at some distance from the source the direct waves will be overcome by the critically refracted waves at the first layer interface. Likewise, at greater distances the waves refracted at deeper layers will overcome those refracted above. Due to its underling assumptions, the method cannot detect velocity inversions with depth. However, some indications of the presence of a velocity inversion or hidden layer may be obtained using interpretation methods (e.g. Palmer, 1981) or well control.

Within the scope of project SCENE thirty sites where strong motion stations are installed have been characterized using this technique. The surveys were performed, in general, within 200 m from the stations and within the same geologic unit, according to geological maps and field inspections. The SCENE shear-wave database also includes a significant amount of shear-wave refraction data available from FCT project NEFITAG using the same methodological approach. We used as shear-wave source a 3 m long wood beam, coupled to the ground with a four-wheel drive, and stricken on both sides by a sledgehammer, in order to allow data corroboration and to eliminate P-wave contamination (Hasbrouck, 1991). Two shots were performed at both ends (minimum offset distance of 1.75 m) of the array and three shots within the array. The recording system consisted of a linear array of 24 40-Hz horizontal receivers and 24 50-Hz vertical receivers spaced 3.5 m apart. The overall length of the array, which constrains the depth reached by the survey, was 84 m.

The data interpretation was performed with commercial software relying on the generalized reciprocal method (Palmer, 1981) and slope intercept method, and the method of Haeni *et al.* (1987). The latter uses delay-times for constraining a first preliminary velocity model, followed by three iterations of ray tracing and minimization of residuals by least squares. The results are a 2-D V_S cross section. Further details on both the survey and data interpretation can be found on Carvalho et al., unpublished report, 2017, see Data and Resources;

A total of 61 V_S depth sections have been acquired using this methodological approach. In general we are confident to have reached 30 m deep in the seismic sections. In many cases we were actually able to identify interfaces deeper than 30 m, which demonstrates that both the source used and the equipment setup allowed for the 30 m to be reached. However, investigation depth depends on the velocity distribution at each site. Therefore, we compared our interpretations with other available information such as borehole data in the vicinity of the profiles. The vertical resolution in seismic refraction data is usually accepted to vary between 10% to 20% of the reflector's depth or one quarter of the wavelength (e.g., Briaud (2013), page 155). Therefore using the described procedure we are not expected to detect layers thinner than around 3 m (except the uppermost layer) and around 6 m at $20 - 30$ m deep. The lateral resolution is typically around 1/2 to 1 of the spacing between receivers, which corresponds to about $2 - 3$ m.

Multichannel Analysis of Surface Waves

The use of surface-wave methodologies to estimate the V_S depth structure of a site relies on the dispersive characteristics of Rayleigh-type surface waves traveling through a heterogeneous medium. The velocity of this type of waves depends on the mechanical properties of the propagation medium. Since lower frequencies and long wavelength waves penetrate deeper into the material than high frequency and short wavelength waves, their velocities will reflect the differences in the mechanical properties of the volumes they travel trough. Because more information is available for the upper layers, these are better constrained than the deeper ones.

The dispersion curve is obtained by converting the data to frequency domain and by identifying the different propagation modes. An inversion algorithm is then applied for obtaining a V_S structure compatible with the experimental dispersion curve. The multichannel analysis of surface wave technique (MASW) (Gabriels *et al.*, 1987; Park *et al.*, 1999) uses an array of receivers to record the seismic wave-field produced by an active source. The refraction microtremor technique (ReMi) (Louie, 2001) employs a similar approach but with passive sources.

In spite of the inherent non-uniqueness associated with MASW results several studies have shown that different profiles that fit a particular dispersion curve lead to similar V_{S30} values (e.g. Comina *et al.*, 2011).

Seven sites have been analyzed using MASW methodology. We used a 10 kg sledgehammer striking a metal plate as source, and the acquisition system was composed of a 48 m long line with 24 vertical 4.6 Hz geophones spaced 2 m apart. Ten shots were performed at both ends of the acquisition line with an offset of 2 m. We used 2 s long recording intervals with a sampling rate of 1 ms. Several separate acquisitions were performed in order to evaluate the uncertainty in determining the dispersion curve. In some cases, considering the geological setting and the site-specific characteristics, different line configurations were tried. The data processing and inversion was performed with the SWAN software (Geostudi Astier) although software Dinver (Wathelet *et al.*, 2004; Wathelet, 2008) was used for comparison. The software SWAN uses an automatic inversion algorithm that allows for an iterative trial and error fit to the dispersion curve. The Dinver algorithm searches the space of solutions by minimizing a misfit curve. The final model was built using the best-fit models together with additional constraints rendered by geological and geotechnical information in the vicinity of the profiles, and some degree of expert judgment with respect to the velocity of the deeper layers.

Invasive Measurements

The seismic cone penetrometer test (SCPTu) is an invasive methodology for directly measuring V_S at specific depths. The probe introduced into the soils contains seismic receiver that records the shear wave travel time from a source located at the surface to the recording depth, as in a downhole test. In four sites located within soft sediments we used SCPTu methodology to determine V_S subsurface structure. We used a single receiver seismic cone and the data was interpreted using the cross-correlation method. The seismic signal was acquired and processed using comercial software provided by the manufacturer of the equipment (See Data and Resources). Measurements were performed every meter until reaching stiff material, which occurred within the depth range of $22 - 26\,\mathrm{m}$.

Other Available Data

We included in the database V_S information available from both the literature and unpublished technical reports using a variety of methodologies: seismic refraction (24 sites, Carvalho *et al.* (2008), Carvalho *et al.* (2009)), MASW (56 sites, Lopes (2005), Lopes *et al.* (2005), Santos (2011), Fontoura (2013), and unpublished surveys performed in the context of service provisions and scientific projects provided by Rui Moura), and ReMi (8 sites, Carvalho *et al.* (2016)). In general, the depths of the profiles included in the database range from $20 - 30\,\mathrm{m}$. However, for some seismic refraction sections the deepest mapped interface is shallower than $15\,\mathrm{m}$, raising questions about the actual depth of the models.

The shear-wave database presently consists of 160 profiles or sections from a variety of lithological/geological formations. From these, about 40% have been acquired within the framework of projects SCENE and NEFITAG, and more than 50% have been estimated using the seismic refraction method. Figure 1b shows the distribution of V_{S30} values in the database. Figure 1c and Figure 1d show, respectively, the geographic distribution of sites sorted by the geologically defined unit and by the methodology used to characterize the V_S depth structure.

Developing the Database Flat-File

In this section we describe the procedures employed in the parametrization of the V_{S30} database. The corresponding flat-file is available as Table S1 in the electronic supplement to this article.

Calculating V_{S30} and Associated Variability

As discussed previously, for seismic refraction data acquired within the scope of projects SCENE and NEFITAG, we are confident that the V_S models extend to 30 m deep. However, since the seismic refraction method maps the interfaces between subsurface layers characterized by different seismic velocities, unless an interface has been actually detected below 30 m, one cannot be totally sure that a depth of 30 m has been reached for a particular section. To evaluate the impact of this uncertainty in the V_{S30} distributions we combined the use of a best-case scenario in which we assumed that all sections reached 30 m (e.g., we assumed constant extrapolation V_{S30C}), with that of a worst-case scenario in which we assumed that the deepest interface roughly corresponds to the maximum depth of the model. In the latter case we use an extrapolation method to obtain V_{S30} from V_{SZ} (V_{S30z}). We used the same approach for profiles whose V_S model is shallower than 30 m. Overall, only about 11% of the profiles are suspected to have depth models that do not reach 15 m deep.

Assuming constant extrapolation down to 30 m deep ($\mathbf{V_{S30c}}$)

To calculate the value of V_{S30} for each site included in the database we proceeded as follows. For seismic refraction sections acquired in the context of projects SCENE and NEFITAG we used the values of the 2D velocity models at the receivers locations and calculated the V_{S30} according to equation (1) assuming that all V_S models reached 30 m depth.

We then calculated the log-average value for the section. We used the log-average instead of the arithmetic mean because of our underlying assumption that V_{S30} follows a lognormal distribution (see section Developing a geologically-based V_{S30} model for Portugal). Using the arithmetic mean leads, however, to very similar values of V_{S30}.

The 2D sections obtained within the scope of previous refraction campaigns (Carvalho *et al.*, 2008, 2009) have been graphically interpolated at five locations within the acquisition line because the original data files have been lost. Then, the same procedure previously described for 2-D sections has been applied. For all available seismic refraction sections we calculated the standard deviation associated with the $\log V_{S30}$ value at each site. This provides a measure of the spatial variability of V_{S30} associated with the sites.

For the MASW-based measurements we calculated the V_{S30} using the preferred final profile, using constant extrapolation when required to reach the depth of 30 m. We calculated the standard deviation of $\log V_{S30}$ at each site by using a set of automatically inverted best-fit profiles as a measure of the variability associated with the methodology.

The log-average has been calculated for the profiles presented by Carvalho *et al.* (2016) for each single site analyzed with the refraction microtremor technique. In this case the associated standard deviation provides a measure of the uncertainty associated with the technique.

At last, for sites analyzed with different methodological approaches, V_{S30} was calculated for each method as described previously and the final V_{S30} value for the site was log-averaged.

In a few sites we had reservations regarding the results of some measurements due to specific difficulties faced during acquisition or analysis. This was the case for seismic refraction section at SC-VFX and multichannel analysis of surface waves profile at SC-BEJ. The corresponding V_S structures were not further considered in the analysis. The standard deviation of $\log V_{S30}$ at sites characterized by multiple techniques provides an estimate of the inter-method variability.

Using Extrapolations Based on $\mathbf{V_{SZ}}$ ($\mathbf{V_{S30z}}$)

We checked the applicability of the relationship proposed by Boore (2004) and Boore *et al.* (2011) to extrapolate V_{S30} from shallower velocity structures, based on data from California and Japan, respectively, to our data. The relationships are based on the parameter V_{SZ}, which represents the time averaged V_S to the depth z, and is given by

$$V_{SZ} = \frac{z}{\sum t_{iz}} \tag{2}$$

where t_{iz} is the travel time within each layer up to the depth z.

We calculated V_{SZ} for profiles reaching 30 m deep for $z = 10, 15, 20,$ and 25 m. In the seismic refraction data we assumed that profiles exhibiting interfaces at depth $z > 25$ m did reach 30 m depth. Refraction profiles that reached high values of V_S, typical of bedrock, have also been included. Profiles obtained with other methodologies were included only if the model explicitly reached a depth of 30 m. V_{S30} is plotted as a function of V_{SZ} in Figure 2, together with the relationships proposed for California (Boore, 2004) and for Japan (Boore *et al.*, 2011). The results indicate that the relationships developed for California are more suited to represent the trends of regional data than those for Japan, in particular in what concerns the shallower depths considered ($z = 10$, and 15 m). We therefore consider the functional forms proposed by Boore (2004) to extrapolate the profiles that may have not reached 30 m depth.

Classifying the Surface Geology

The site classification was performed using the 1:50.000 scale geological maps published by Serviços Geológicos de Portugal. If that scale was not available we used the 1:200.000 scale geological maps. In few locations the only available geological map was at the 1:500.000 scale.

The consistency of the maps was a problem in particular for the southernmost region of Portugal. In some cases the same unit was attributed a different geological age in adjacent maps. We corrected the units according to the 1:200.000 scale geological map, which was consistent throughout the region, and a comment was introduced in the flat-file. This type of inconsistency has been also reported by Stewart *et al.* (2014) for Greece.

Calculating the Topographic Slope

Following Wald and Allen (2007) we calculated the topographic-slope associated with each site in the database using the Generic Mapping Tools slope function *grdgradient*; Wessel and Smith (1991). We used freely available topographic data sets from the Shuttle Radar Topography Mission at 30 arcsec resolution (SRTM30) and at 3 arcsec resolution (SRTM3)(see Data and Resources). The topographic-slope value for each site was calculated using the nearest neighbor interpolation.

Developing a geologically-based V_{S30} model for Portugal

In this section we describe the methodological approach used for deriving a V_{S30} site condition model for Portugal using extrapolation based on surface geology. Our objective was to estimate the most accurate model statistically supported by the dataset. To accomplish this goal we followed an iterative three-step procedure which consisted of 1) defining a preliminary set of geologically defined units based on the literature; 2) estimating the probability distribution of $\log V_{S30}$ for each of those units; and 3) performing statistical tests in order to estimate the statistical significance of the difference in the $\log V_{S30}$ distribution characteristics between the units. The units were merged according to the results of the statistical tests and the procedure was repeated.

It has been debated whether V_{S30} or the (decimal) logarithm of V_{S30} ($\log V_{S30}$) should be used as the variable for deriving V_{S30} predicting models. (e.g., Lemoine *et al.*, 2012). The use of $\log V_{S30}$ as a variable assumes that V_{S30} observations follow a lognormal distribution (e.g., Park and Elrick, 1998; Ashland and McDonald, 2003). Boore *et al.* (2011) show that, unlike V_{S30}, $\log V_{S30}$ values in their database follow a normal distribution. This is also the case for our dataset as can be graphically illustrated by the quantile-quantile plot in Figure 3. Since most statistical tests require that data are normally distributed we used $\log V_{S30}$ as the dependent variable in our model.

The preliminary model consisted of six preliminary geologically defined units that are summarized in Table 1. We used as variables V_{S30c}, in which we assumed constant extrapolation for all profiles, and V_{S30z}, in which we used the functional forms proposed by Boore (2004) to extrapolate the profiles that did not or may have not reached 30 m depth. Figure 4 shows histograms for $\log V_{S30c}$ together with fitted normal distributions for both $\log V_{S30c}$ and $\log V_{S30z}$. The dataset is not, in general, significantly affected by uncertainty regarding the extrapolation method for profiles that may have not reached 30 m depth. The unit most affected by this type of uncertainty is P4 (Pliocene formations). The dispersion of data is similar and around 0.2 for every geologically defined unit except P4 ($\sigma = 0.1$). This issue may be related with the relatively lower lithological variety associated with the Pliocene age in the region. However, more data is necessary in order to confirm this hypothesis. In general the $\log V_{S30}$ distributions for each geologically defined unit do not show systematic trends with the data's geographical region.

Declustering

Attributes measured in clustered datasets may not be representative of those of the population since closely spaced observations may exhibit strong spatial autocorrelation (e.g., De Smith *et al.*, 2015). This issue is particularly relevant for cases where preferential sampling applies. In preferential sampling a large number of observations are spatially aggregated in regions of interest, where the variable to be analyzed is expected to take consistently high or low values. In these cases population attributes such as the mean values, standard deviation will probably be substantially biased.

The database developed for this study includes shear-wave profiles acquired in the context of research projects with different aims. For project SCENE, the adopted strategy of acquiring data in the vicinity of sites where strong-motion instruments were installed led to a dataset that is spatially disperse. That is also the case for project NEFITAG, and data from Carvalho *et al.* (2008, 2009, 2016) whose data-acquisition policy aimed at sampling different geological units within relatively large regions. However, in other studies, a relatively small region was extensively sampled, producing datasets that exhibit strong spatial clustering. In particular, data from Santos (2011) are probably affected by preferential sampling since the aim of that study was to map the thickness of altered rocks.

Declustering methods are based on the weighting of the sample data in order to account for spatial representativity. Closely spaced observations receive a reduced weight because of its redundancy. Cell declustering and polygonal declustering are the most widely used declustering methods (e.g., Olea, 2007). In polygonal declustering the domain is divided into polygons that define the area of influence of each observation and the attributed weights are proportional to that area. This method has the disadvantage of being extremely sensitive to the location of the domain boundaries (e.g., Olea, 2007; De Smith *et al.*, 2015). In cell declustering (Journel, 1983; Deutsch, 1989; Deutsch and Journel, 1992) a regular grid of cells is superimposed over the data domain and the attributed weights are inversely proportional to the number of observations per cell. Deutsch (2015) discusses the parametrization for cell declustering and proposes that the cell size should be related to the spacing of data in sparse sampled areas. A set of randomly selected locations is usually used for the origin of the cell grid.

We evaluated the extent to which spatial clustering or preferential sampling affects the mean value of $\log V_{S30}$. We compared the histograms calculated from both the full dataset and a dataset obtained by using the cell declustering technique. The cell size was chosen on the basis of the average nearest neighbor distance for the sparse areas of the dataset. Cell sizes of 10 km, 15 km and 20 km have been tested with similar results. For each grid size a randomly selected set of 10 grid origins have been used. A square grid size of 10 km was retained for the final analysis.

Figure 4 shows the fitted normal distributions for the declustered dataset. The normal distribution fitted to generalized geologic unit P1 shows a significant degree of bias that may be attributed to spatial clustering or preferential sampling. However, the attributes of the remaining generalized geological units are not significantly affected by declustering. For the subsequent analysis we used a declustered version of the dataset assigned to geologic unit P1.

Statistical Tests

The analysis of variance (ANOVA) is a statistical test that is used for assessing whether there are statistical significant differences between the means of a set of independent groups. The method relies on computing the F value, which is the ratio between the variances within and between groups, and determining the corresponding F-distribution under the null hypothesis that data from all groups belong to a common distribution function. A p-value determined from the F-distribution reflects the probability that the calculated F value has occurred by chance. The ANOVA test assumes that 1) the samples are independent, 2) the underlying populations are normally distributed, and 3) the variance of data in groups are homogeneous. Unlike using multiple t-tests, the ANOVA procedure ensures that the final significance level is achieved. If the null hypothesis is rejected one can proceed the analysis using a post-hoc test such as the Tukey-HSD (Honestly Significant Difference). The Tukey-HSD approach uses the Studentized Range distribution to evaluate which group's means are significantly different from each other. The test computes the value q, which is the difference between the means divided by the standard deviation, for all pairwise comparisons. The corresponding p-value is obtained by comparing that value with Studentized Range distribution for the null hypothesis.

Results

We tested the null hypothesis for the independent variable $\log V_{S30}$ distributed by six groups, corresponding to the preliminary set of geologically defined units. The resulting F value of 22.9467 corresponds to a P-value of 2.5e$-$15, much below the common significance level of 5%. Therefore we reject the null hypothesis and proceed the post-hoc analysis using the Tukey-HSD method. The results for the Tukey-HSD test for the preliminary model are summarized in Table 2.

The Tukey-HSD post-hoc test results indicate that there is no statistically significant difference between groups P1 and P2 and between groups P3, P4 and P5, and to a lesser extent between groups P2 and P3 and P2 and P5. We merged the groups exhibiting higher values for p-value and repeated the procedure. The resulting set of groups of geological units defined by the tests – F1, F2 and F3 – are summarized in Table 3. The results of the statistical tests for F1, F2 and F3 are presented in Table 2. The ANOVA test produced a F value of 57.4279 which corresponds to a p-value of $1e^{-16}$. The ensuing Tukey-HSD test indicates that the difference in the means of the groups is statistically significant.

The final model is illustrated in Figures 5 and 6. The median V_{S30} values for the geologically defined units F1, F2 and F3 are 829 m/s, 470 m/s and 237 m/s, respectively. However, the 68% confidence interval for V_{S30} overlaps for F1 and F2 and for F2 and F3, i.e, the lower limit for F1 is lower than the upper limit for F2, and the lower limit for F2 is lower than the upper limit for F3. This is partially related to the inherent limitations of surface geology as a predictor for V_{S30}. A geologically defined unit includes different rock types, lithologies and layer thicknesses, which influence the VS depth structure and consequently the corresponding V_{S30} value. Other geologically-based V_{S30} models display similar dispersion values despite the fact of presenting more specific geologically defined units (Wills and Clahan, 2006). Nevertheless, some dispersion could be related to the limited size of the database. A larger dataset that would allow the definition of more specific geologically defined units or the inclusion of other geographic criteria (e.g., Holocene in narrow valleys, small basins, etc.), might eventually decrease the dispersion within some units.

Relationship with Topographic-Slope

We investigated the relationship between topographic slope and $\log V_{S30}$ in order to evaluate the extent to which that variable could be used to refine the V_{S30} model. Figure 7 shows $\log V_{S30}$ as a function of topographic slope for both the SRTM30 and SRTM3 elevation datasets, sorted by the final set of generalized geological units F1, F1 and F3. The relationship between V_{S30} and topographic slope is in general extremely poor for the SRTM30 dataset, regardless of the geological unit. There is however a slight tendency for some F3 sites to concentrate in the lower-left part of the graphic (lower V_{S30} corresponding to lower slope). The SRTM3 dataset shows a much clearer correlation between those two variables for F3 sites only. Tentative V_{S30}-slope classes for F3 sites are outlined in Figure 7b). A t-test run indicates that the differences in V_{S30} distributions pertaining to the topographic slope classes 0.002m/m $< slope <$ 0.016m/m 0.016m/m $< slope <$ 0.100m/m are statistically significant at a 5% confidence level (pvalue=0.08). However, since the sample sizes are fairly small (less than 15) the statistical power of the result is low, which means that there is a reduced likelihood that a statistically significant result reflects a true effect.

Evaluation of Proxies Based on Exogenous Data

In the absence of local V_{S30} data is is common practice to estimate that variable using proxies derived from data pertaining to other regions. We used the database developed in this study to evaluate the performance of V_{S30} proxies proposed in the literature. The topographic-slope is the most widely used V_{S30} proxy (Wald and Allen, 2007). The model relies on correlations between the topographic-slope calculated for the SRTM30 elevation data set and V_{S30} data from California, Utah, Central United States, Taiwan, Italy and Australia. We use the model as implemented in the global V_{S30} server (Allen and Wald (2007); see Data and Resources).

In the geologic analogue proxy approach, local geologic units are correlated with geologic categories developed in a different geographic context, which are characterized by V_{S30} distributions. Vilanova *et al.* (2012) used the geologically-based V_{S30} model developed by Wills and Clahan (2006) for California as a proxy for estimating V_{S30} at sites, in Portugal, where ground motion stations were deployed. It has been shown by Stewart *et al.* (2008) that Wills and Claham's (2006) model had no significant bias with respect to V_{S30} distributions for geologic units in Italy. Vilanova *et al.* (2012) used Stewart *et al.* (2008) V_{S30} distributions for estimating V_{S30} for geologic conditions that do not have geological analogue in California.

Silva *et al.* (2015) likewise used both the geologically-based V_{S30} models of Wills and Clahan (2006) and Stewart *et al.* (2008) to estimate the site conditions for Portugal. They selected, however, dissimilar geological analogues with respect to Vilanova *et al.* (2012) for the local geological units. For instance, Silva *et al.* (2015) used "Quaternary (Pleistocene) sand deposits" ($V_{S30} = 302 \pm 46$m/s) as the geological analogue for "Sandstones, more or less argillaceous limestone, sands, gravels, clays, from Miocene and Pliocene", while Vilanova *et al.* (2012) correlated that unit with "Tertiary sandstone units" ($V_{S30} = 515 \pm 215$m/s). This example illustrates the difficulties associated with implementing V_{S30} proxies based on the geological analogue methodological approach.

Figure 8 shows the residual distributions for $\log V_{S30}$, for both the proxy model based on slope and that based on the geological analogues. We used the Silva *et al.* (2015) geologically-based model because since it applies to the most extensively representative geological units of Portugal, the exercise corresponds to a truly blind comparison.

The use of proxies based either on geological analogues or on correlations with the topographic slope shows fairly unbiased total residual distributions of $\log V_{S30}$. However, the performance of the methods varies significantly with the generalized geological unit analyzed. The topographic-slope proxy is biased towards lower values of V_{S30} for F1 sites (Igneous, metamorphic and old sedimentary rocks) and it is biased towards higher values of V_{S30} for F3 sites (Holocene formations). It is unbiased for the most extensive dataset which pertains to F2 sites (Neogene and Pleistocene formations). The residual's distribution shows clear linear trends with the independent variable (topographic-slope) for all geological categories. The residuals are positive for lower values of $\log V_{S30\text{slope}}$ and negative for higher values of topographic slope, indicating that the relationship between V_{S30} and topographic-slope assumed by the model doesn't apply to the three subsets.

The geological analogue model of Silva *et al.* (2015) is slightly biased for sites located both on F1 and F3 geological units (Igneous, metamorphic and old sedimentary rocks, and Holocene formations, respectively). It is however strongly biased towards lower values of V_{S30} for F2 sites (Neogene and Pleistocene formations). This is probably related to the fact that Pleistocene formations in our dataset display $\log V_{S30}$ distributions similar to those of Neogene, with a mean value higher than what would be expected from the model of Wills and Clahan (2006). In addition, the fact that Silva *et al.* (2015) considered some Miocene and Pliocene formations correlated with Pleistocene formations in California, also contributed to exacerbating the bias.

Discussion and Conclusions

We developed a V_{S30} database for Portugal, by acquiring and gathering of V_S profiles using different techniques. Most of the sites in the database have been characterized in terms of V_S depth profile using the seismic refraction technique. Other techniques used include MASW, seismic cone penetrometer and ReMi. Few sites tested using different techniques showed in general compatible V_S depth profiles and corresponding V_{S30} values.

We present a geologically-based V_{S30} model for Portugal, which includes three geological categories: F1 - Igneous, metamorphic, and sedimentary rocks of Mezosoic or Paleogene age; F2 - Neogene and Pleistocene Formations; and F3 - Holocene Formations. The $\log V_{S30}$ distributions pertaining to each geologic category are statistically significantly different from each other.

The methodological approach used for developing this model involves an iterative three-step procedure which consists of: 1) Defining a preliminary set of geologically defined units based on the literature; 2) calculating the $\log V_{S30}$ distribution for each geologically defined unit; and 3) merging the units according to the results of statistical testing.

We investigated the correlation between $\log V_{S30}$ and topographic-slope in order to evaluate the extent to which the last could be used as a variable for refining the model. The topographic-slope has been successfully used for this purpose by Thompson *et al.* (2014) and Stewart *et al.* (2014).

We find that, in general, and in what concerns our dataset, the correlation between slope and V_{S30} is poor. The relationship is similar to that reported by Lemoine *et al.* (2012) for stable continental regions within Europe, with slope values ranging between $0.05 - 0.10$m/m, regardless of the $\log V_{S30}$ value. Part of the F3 sites (Holocene formations) in our dataset tends, however, to display lower topographic-slope values than the remaining geological defined units. This becomes more evident using SRTM3 elevation dataset for calculating the topographic-slope than using the SRTM30 dataset. In this case the topographic slope can be used to refine the model for F3 sites. However, because the sample sizes are relatively small, this issue needs to be further investigated whenever a larger dataset pertaining to F3 is available. The correlation between topographic-slope and V_{S30} for Holocene formations is probably related to the relationship between the sedimentation environment and grain size.

Stewart *et al.* (2014) also reported that the topographic slope calculated using the SRTM3 dataset reveled better correlation with V_{S30} than either higher or lower resolution digital elevation models. The decrease in performance with higher than 3 arc seconds resolution elevation models has been attributed to canopy effects (Allen and Wald, 2009; Stewart *et al.*, 2014).

We believe that our final model, although relatively broad, is the best that can be achieved with the currently available dataset. Whenever a larger dataset is available, it may be possible to develop a better model, both in terms of accuracy and precision, without compromising the corresponding statistical robustness.

The underlying dataset presents several important limitations. In particular, some data are heavily clustered, some geological units are poorly sampled, and some geographical regions are underrepresented. This database will be used to assist the selection of future sites to be characterized in terms of V_S depth distribution. For instance Holocene formations along the western coast and small basins need to be better sampled in the future. The $\log V_{S30}$ distributions show, however, no evidence of systematic trends with geographic location, suggesting that those limitations in the dataset do not significantly affect the results.

We evaluated the performance of models for V_{S30} developed from proxies, such as topographic-slope or surface geology, with data coming from exogenous regions. We used the model based on topographic-slope as implemented by Allen and Wald (2007) and the model based on geologic analogues with the model by Wills and Clahan (2006) for California as implemented by Silva *et al.* (2015). Both models display overall unbiased residuals between estimated and measured V_{S30} values. However their performance relative to data pertaining to each geologically defined unit is highly irregular. The model based on topographic slope is unbiased for F2 sites, but strongly biased for both F1 and F3 sites. We find that the model based on topographic-slope presents, overall, spurious spatial variations of V_{S30}. A positive point about this methodology is that it seems to effortlessly be able to partially identify F3 sites, which are in general characterized by lower values of V_{S30} with respect to F1 and F2 sites.

The model based on geological analogues is fairly unbiased for both F1 and F3 sites, but is severely biased for F2 sites. This bias is in part related to the challenges associated with correlating geological units from regions with different geological and lithological conditions. Due to these difficulties, the usefulness of this model in estimating V_{S30} should be regarded in a qualitative sense only.

We conclude that in the absence of endogenous data the method based on analogue surface geology units should be preferred to that based on topographic-slope. We stress however that topographic-slope may be useful in identifying Holocene basins in the absence of more pertinent data. Both proxies should be regarded as supplying qualitative information on the distributions of V_{S30}, emphasizing the need for acquiring regional V_S data.

Data and Resources

The database (flat-file) used in this paper is available as Table S1 in the electronic supplement to the paper. The digital elevation models used, the 3-arcsec resolution (SRTM3) and the 30-arcsec resolution (SRTM30) datasets, were obtained respectively at http://srtm.csi.cgiar.org, last accessed June 2017, and https://dds.cr.usgs.gov/srtm/version2_1/SRTM30/, last accessed June 2017.

The global V_{S30} model based on slope is available at https://earthquake.usgs.gov/data/vs30, last accessed June 2017.

We used the ISC Catalogue (ISC, 2014) for plotting the seismicity: International Seismological Centre (2014), On-line Bulletin., Internatl. Seismol. Cent., Thatcham, United Kingdom, available at http://www.isc.ac.uk, last accessed January 2017.

The figures were plotted using the Generic Mapping Tools package developed by Paul

Wessel and Walter Smith (https://www.soest.hawaii.edu/gmt/), last accessed June 2017, and the QGIS 2.6.1 Geographic information System, Open Source Geospatial Foundation Project (http://qgis.osgeo.org), last accessed June 2014.

The SCPTu data was acquired and interpreted using the software provided by the manufacturer (Pagani Geotechnical Equipment, http://www.pagani-geotechnical.com, last accessed October 2017).

The following reference is in the process of publication: "Near surface characterization of the Lisbon and Lower Tagus Valley area, Portugal, for seismic hazard assessment: V_{S30} and soil classification maps" by J. Carvalho, R. Dias, R. Ghose, J. Borges, J. Narciso, C. Pinto, and J. Leote.

Acknowledgements

The Portuguese Foundation for Science and Technology (FCT) funded this work through research projects SCENE (PTDC-CTE/GIX/103032/2008), NEFITAG (PTDC-CTE/GIX /102245/2008), SEICHE (EXCL/GEO-FIQ/0411/2012) and SHARPE (IF-EXPLOR). S.P.V. acknowledges FCT for her contract IF/01561/2014/CP1214/CT0006 under IF2014 Program. CERENA research unit is funded by FCT through strategic project UID/ECI/04028/2013.

Joana Carvalho kindly supplied the refraction microtremor depth profiles from the Carvalho *et al* (2016) study, and Ana Paula Falco provided assistance in GIS-related issues.

Finally, we would like to acknowledge Editor Thomas Pratt, Associate Editor Mark Stirling and two anonymous reviews for their valuable comments that helped us improving and clarifying the manuscript.

References

Aki, K., and P. G. Richards (1980). *Quantitative Seismology*, volume 1. W. H. Freeman, San Francisco, CA, USA.

Allen, T. I., and D. J. Wald (2007). Topographic slope as a proxy for seismic site-conditions (V_{S30}) and amplification around the globe. *Open-File Report 2007-1357*, U.S. Geol. Surv.

Allen, T. I., and D. J. Wald (2009). On the use of high-resolution topographic data as a proxy for seismic site conditions (V_{S30}). *Bull. Seismol. Soc. Am.* **99** 935–943.

Ashland, F. X., and G. N. McDonald (2003). Interim map showing shear-wave-velocity characteristics of engineering geologic units in the salt lake city, utah, metropolitan area. *Open-File Report 424*, Utah Geological Survey, Utah Department of Natural Resources.

Boore, D. M. (2004). Estimating $V_s(30)$ (or NEHRP site classes) from shallow velocity models (depths $<$ 30 m). *Bull. Seismol. Soc. Am.* **94** 591–597.

Boore, D. M., and M. W. Asten (2008). Comparisons of shear-wave slowness in the Santa Clara Valley, California, using blind interpretations of data from invasive and noninvasive methods. *Bull. Seismol. Soc. Am.* **98** 1983–2003.

Boore, D. M., E. M. Thompson, and H. Cadet (2011). Regional correlations of V_{S30} and velocities averaged over depths less than and greater than 30 meters. *Bull. Seismol. Soc. Am.* **101** 3046–3059.

Borcherdt, R. D. (1994). Estimates of site-dependent response spectra for design (methodology and justification). *Earthq. Spectra* **10** 617–653.

Briaud, J-L. (2013). *Geotechnical Engineering: Unsaturated and Saturated Soils.* John Wiley & Sons, New Jersey, USA.

Building Seismic Safety Concil (BSSC) (2004). NEHRP recommended seismic provisions for new buildings and other structures (FEMA 450), Part 1: Provisions. *2003 Edition*, Building Seismic Safety Council, National Institute of Building Sciences, Washington D.C.

Cadet, H., P.-Y. Bard, and A. Rodriguez-Marek (2010). Defining a standard rock site: Propositions based on the kik-net database. *Bull. Seismol. Soc. Am.* **100** 172–195.

Canora, C., S. P. Vilanova, G. M. Besana-Ostman, J. Carvalho, S. Heleno, and J. Fonseca (2015). The Eastern Lower Tagus Valley Fault Zone in central Portugal: Active faulting in a low-deformation region within a major river environment. *Tectonophysics* **660** 117–131.

Carvalho, J., L. Torres, R. Castro, R. Dias, and L. Mendes-Victor (2009). Seismic velocities and geotechnical data applied to the soil microzoning of western Algarve, Portugal. *J. Appl. Geophys.* **68** 249–258.

Carvalho, J. F., P. Teves-Costa, L. Almeida, and I. M. Almeida (2016). Seismic susceptibility map for Cascais County (Portugal): a simple approach. *Bull. Eng. Geol. Environ.* **75** 1227–1249.

Carvalho, J. P., R. P. Dias, C. C. Pinto, J. Leote, and L. M. Victor (2008). A soil classification for seismic hazard assessment and mitigation of the Algarve. In *The 14th World Conference on Earthquake Engineering, October 12-17, 2008.* 9.

Castellaro, S., F. Mulargia, and P. L. Rossi (2008). V_{S30}: Proxy for seismic amplification? *Seismol. Res. Lett.* **79** 540–543.

CEN (2004). *Eurocode 8: design of structures for earthquake resistance – part 1: general rules, seismic actions and rules for buildings.* European Committee for Standardization, Brussels, Belgium.

Comina, C., S. Foti, D. Boiero, and L. V. Rossi (2011). Reliability of $V_{S,30}$ Evaluation from surface-wave tests *J. Geotech Geoenviron* **137** 579–586.

Custódio, S., N. A. Dias, F. Carrilho, E. Góngora, I. Rio, C. Marreiros, I. Morais, P. Alves, and L. Matias, (2015). Earthquakes in western Iberia: improving the understanding of lithospheric deformation in a slowly deforming region. *Geophys. J. Int.* **203** 127–145.

De Smith, M. J., M. F. Goodchild, and P. Longley (2015). *Geospatial analysis: a comprehensive guide to principles, techniques and software tools*. The Winchelsea Press, Winchelsea, UK.

Deutsch, C. (1989). DECLUS: a FORTRAN 77 program for determining optimum spatial declustering weights. *Computers & Geosciences* **15** 325–332.

Deutsch, C. V. (2015). Cell declustering parameter selection. In J. L. Deutsch (Editor), *Geostatistics Lessons*, Centre for Computational Geostatistics. 6.

Deutsch, C. V., and A. G. Journel (1992). *GSLlB, Geostatistical software library and user's guide*. Oxford University Press.

Fonseca, J. F. (2005). The source of the Lisbon earthquake. *Science* **308** 50–50.

Fontoura, M. J. d. S. (2013). *Estudo geológico e geofísico da dispersão de contaminantes em vazadouro controlado de resíduos sólidos urbanos na área metropolitana do Porto*. Ph.D. thesis, Faculdade de Ciências da Universidade do Porto.

Fukao, Y. (1973). Thrust faulting at a lithospheric plate boundary the Portugal earthquake of 1969. *Earth Planet. Sci. Lett.* **18** 205–216.

Gabriels, P., R. Snieder, and G. Nolet (1987). In situ measurements of shear-wave velocity in sediments with higher-mode rayleigh waves. *Geophys. Prospect.* **35** 187–196.

Haeni, F., D. G. Grantham, and K. Ellefsen (1987). Microcomputer-based version of SIPT; a program for the interpretation of seismic-refraction data. *Open-File Report 87-103*, U.S. Geol. Surv.

Hasbrouck, W. P. (1991). Four shallow-depth, shear-wave feasibility studies. *Geophysics* **56** 1875–1885.

Hassani, B., and G. M. Atkinson (2016). Site-effects model for Central and Eastern North America based on peak frequency. *Bull. Seismol. Soc. Am.* **106** 2197–2213.

Iwahashi, J., and R. J. Pike (2007). Automated classifications of topography from DEMs by an unsupervised nested-means algorithm and a three-part geometric signature. *Geomorphology* **86** 409–440.

Johnston, A. C. (1989). The seismicity of 'Stable Continental Interiors'. In *Earthquakes at North-Atlantic Passive Margins: Neotectonics and Postglacial Rebound*, Springer. 299–327.

Johnston, A. C. (1996). Seismic moment assessment of earthquakes in stable continental regions—III. New Madrid 1811–1812, Charleston 1886 and Lisbon 1755. *Geophys. J. Int.* **126** 314–344.

Journel, A. G. (1983). Nonparametric estimation of spatial distributions. *Math. Geol* **15** 445–468.

Joyner, W. B., R. E. Warrick, and T. E. Fumal (1981). The effect of Quaternary alluvium on strong ground motion in the Coyote Lake, California, earthquake of 1979. *Bull. Seismol. Soc. Am.* **71** 1333–1349.

Kamai, R., N. A. Abrahamson, and W. J. Silva (2016). V_{S30} in NGA GMPEs-regional differences and suggested practice. *Earthq. Spectra* **32** 2083–2108.

Kramer, S. L. (1996). *Geotechnical earthquake engineering*. Prentice Hall, Upper Sad River, NJ, USA.

Lemoine, A., J. Douglas, and F. Cotton (2012). Testing the applicability of correlations between topographic slope and V_{S30} for Europe. *Bull. Seismol. Soc. Am.* **102** 2585–2599.

Lopes, I., J. Santos, and I. Almeida (2005). Use of surface waves for geotechnical characterization of soft alluvial deposits – the Póvoa de Santa Iria case study. *Near Surf. Geophys.* **3** 47–56.

Lopes, I. M. F. (2005). *Caracterização geotécnica de solos no domínio das pequenas deformações: aplicação do método das ondas superficiais.* Ph.D. thesis, Faculdade de Ciências da Universidade de Lisboa, Lisbon, Portugal.

Louie, J. N. (2001). Faster, better: shear-wave velocity to 100 meters depth from refraction microtremor arrays. *Bull. Seismol. Soc. Am.* **91** 347–364.

Martínez Solares, J., and A. López Arroyo (2004). The great historical 1755 earthquake. effects and damage in Spain. *J. Seismolog.* **8** 275–294.

McDonald, G. N., and F. X. Ashland (2008). Earthquake site conditions in the Wasatch Front corridor, Utah. *Special Study 125*, Utah Geological Survey, Utah Department of Natural Resources.

Moss, R. E. S. (2008). Quantifying measurement uncertainty of thirty-meter shear-wave velocity. *Bull. Seismol. Soc. Am.* **98** 1399–1411.

Motazedian, D., J. Hunter, A. Pugin, and H. Crow (2011). Development of a V_{S30} (NEHRP) map for the city of Ottawa, Ontario, Canada. *Canadian Geotechnical Journal* **48** 458–472.

Olea, R. A. (2007). Declustering of clustered preferential sampling for histogram and semivariogram inference. *Math. Geol* **39** 453–467.

Palmer, D. (1981). An introduction to the generalized reciprocal method of seismic refraction interpretation. *Geophysics* **46** 1508–1518.

Park, C. B., R. D. Miller, and J. Xia (1999). Multichannel analysis of surface waves. *Geophysics* **64** 800–808.

Park, S., and S. Elrick (1998). Predictions of shear-wave velocities in southern California using surface geology. *Bull. Seismol. Soc. Am.* **88** 677–685.

Pinheiro, L., R. Wilson, R. Pena dos Reis, R. Whitmarsh, and A. Ribeiro (1996). The western Iberia margin: a geophysical and geological overview. In *Proceedings-ocean Drilling Program Scientific Results*. National Science Foundation, 3–26.

Pinto, F. D. F. (2013). *Avaliação dos Efeitos Locais para a Estimativa da Perigosidade Sísmica a Nível Nacional.* Master's thesis, Instituto Superior Técnico, Universidade Técnica de Lisboa, Lisbon, Portugal.

Reiter, L. (1990). *Earthquake hazard analysis: issues and insights.* Columbia University Press, New York, NY, USA.

Ribeiro, A., M. Antunes, M. Ferreira, R. Rocha, A. Soares, G. Zbyszewski, F. Moitinho de Almeida, D. Carvalho, and J. Monteiro (1979). *Introduction à la Géologie generale du Portugal.* Serviços Geológicos de Portugal.

Rockwell, T., J. Fonseca, C. Madden, T. Dawson, L. A. Owen, S. Vilanova, and P. Figueiredo (2009). Palaeoseismology of the Vilariça segment of the Manteigas-Bragança fault in northeastern Portugal. *Geological Society, London, Special Publications* **316** 237–258.

Santos, P. (2011). *Cartografia de Espessura de Alteração numa Zona Piloto da Margem do Douro através de Métodos Sísmicos: Implicações para o Ordenamento do Território.* Ph.D. thesis, Faculdade de Ciências da Universidade do Porto.

Scott, J. B., T. Rasmussen, B. Luke, W. J. Taylor, J. Wagoner, S. B. Smith, and J. N. Louie (2006). Shallow shear velocity and seismic microzonation of the urban Las Vegas, Nevada, Basin. *Bull. Seismol. Soc. Am.* **96** 1068–1077.

Serviços Geológicos de Portugal (1992). Carta geológica de portugal.

Silva, V., H. Crowley, H. Varum, and R. Pinho (2015). Seismic risk assessment for mainland Portugal. *Bull. Earthquake Eng.* **13** 429–457.

Stein, S., and M. Wysession (2009). *An introduction to seismology, earthquakes, and earth structure.* Blackwell Publishing Ltd., Malden, MA, USA.

Stewart, J. P., S.-J. Chiou, J. D. Bray, R. W. Graves, P. G. Somerville, and N. A. Abrahamson (2001). Ground motion evaluation procedures for performance-based design. *Peer 2001/09*, Pacific Earthquake Engineering Research Center, Berkeley, USA.

Stewart, J. P., N. Klimis, A. Savvaidis, N. Theodoulidis, E. Zargli, G. Athanasopoulos, P. Pelekis, G. Mylonakis, and B. Margaris (2014). Compilation of a local V_S profile database and its application for inference of V_{S30} from geologic-and terrain-based proxies. *Bull. Seismol. Soc. Am.* **104** 2827–2841.

Stewart, J. P., G. Scasserra, G. Lanzo, F. Mollaioli, and P. Bazzurro (2008). Critical evaluation of Italian strong motion data and comparison to NGA ground motion prediction equations. *UCLA SGEL Report 2008/03*, Department of Civil & Environmental Engineering, University of California, Los Angeles, USA.

Stucchi, M., A. Rovida, A. G. Capera, P. Alexandre, T. Camelbeeck, M. Demircioglu, P. Gasperini, V. Kouskouna, R. Musson, M. Radulian, K. Sesetyan, S. Vilanova, D. Baumont, H. Bungum, D. Fäh, W. Lenhardt, K. Makropoulos, J. M. Martinez Solares, O. Scotti, M. Živčić, P. Albini, J. Batllo, C. Papaioannou, R. Tatevossian, M. Locati, C. Meletti, D. Viganò, and D. Giardini (2013). The SHARE European earthquake catalogue (SHEEC) 1000–1899. *J. Seismolog.* **17** 523–544.

Thompson, E., D. J. Wald, and C. Worden (2014). A V_{S30} map for California with geologic and topographic constraints. *Bull. Seismol. Soc. Am.* **104** 2313–2321.

Thompson, E. M., L. G. Baise, and R. E. Kayen (2007). Spatial correlation of shear-wave velocity in the San Francisco Bay Area sediments. *Soil Dyn. Earthquake Eng.* **27** 144–152.

Tinsley, J., and T. Fumal (1985). Mapping quaternary sedimentary deposits for areal variations in shaking response. *USGS Profess. Pap 1360*, U.S. Geol. Surv., Washington D.C.

Vilanova, S. P., and J. F. Fonseca (2007). Probabilistic seismic-hazard assessment for Portugal. *Bull. Seismol. Soc. Am.* **97** 1702–1717.

Vilanova, S. P., J. F. Fonseca, and C. S. Oliveira (2012). Ground-motion models for seismic-hazard assessment in Western Iberia: Constraints from instrumental data and intensity observations. *Bull. Seismol. Soc. Am.* **102** 169–184.

Vilanova, S. P., C. F. Nunes, and J. F. Fonseca (2003). Lisbon 1755: a case of triggered onshore rupture? *Bull. Seismol. Soc. Am.* **93** 2056–2068.

Wald, D. J., and T. I. Allen (2007). Topographic slope as a proxy for seismic site conditions and amplification. *Bull. Seismol. Soc. Am.* **97** 1379–1395.

Wathelet, M. (2008). An improved neighborhood algorithm: Parameter conditions and dynamic scaling. *Geophys. Res. Lett.* **35** n/a–n/a. L09301.

Wathelet, M., D. Jongmans, and M. Ohrnberger (2004). Surface-wave inversion using a direct search algorithm and its application to ambient vibration measurements. *Near Surf. Geophys.* **2** 211–221.

Wessel, P., and W. H. Smith (1991). Free software helps map and display data. *Eos, Transactions American Geophysical Union* **72** 441–446.

Williams, R. A., W. J. Stephenson, and J. K. Odum (2003). Comparison of P-and S-wave velocity profiles obtained from surface seismic refraction/reflection and downhole data. *Tectonophysics* **368** 71–88.

Wills, C., and K. Clahan (2006). Developing a map of geologically defined site-condition categories for California. *Bull. Seismol. Soc. Am.* **96** 1483–1501.

Wills, C., M. Petersen, W. Bryant, M. Reichle, G. Saucedo, S. Tan, G. Taylor, and J. Treiman (2000). A site-conditions map for California based on geology and shear-wave velocity. *Bull. Seismol. Soc. Am.* **90** S187–S208.

Wills, C. J., and W. Silva (1998). Shear-wave velocity characteristics of geologic units in California. *Earthq. Spectra* **14** 533–556.

Woessner, J., D. Laurentiu, D. Giardini, H. Crowley, F. Cotton, G. Grünthal, G. Valensise, R. Arvidsson, R. Basili, M. B. Demircioglu, S. Hiemer, C. Meletti, R. W. Musson, A. N. Rovida, K. Sesetyan, M. Stucchi, and The SHARE Consortium (2015). The 2013 European seismic hazard model: key components and results. *Bull. Earthquake Eng.* **13** 3553–3596.

Xia, J., R. D. Miller, C. B. Park, J. A. Hunter, J. B. Harris, and J. Ivanov (2002). Comparing shear-wave velocity profiles inverted from multichannel surface wave with borehole measurements. *Soil Dyn. Earthquake Eng.* **22** 181–190.

Yong, A., S. E. Hough, J. Iwahashi, and A. Braverman (2012). A terrain-based site-conditions map of California with implications for the contiguous United States. *Bull. Seismol. Soc. Am.* **102** 114–128.

Full mailing address for each author

Susana P. Vilanova: Centro de Recursos Naturais e Ambiente, Instituto Superior Tcnico, Universidade de Lisboa, Lisbon, Portugal.

João Narciso: Centro de Recursos Naturais e Ambiente, Instituto Superior Tcnico, Universidade de Lisboa, Lisbon, Portugal.

João Carvalho: LNEG,Estrada da Portela-Zambujal, apartado 7586-Alfragide, 2610-999 Amadora, Portugal.

Isabel Lopes: TPF Planege Cenor and CERIS, Instituto Superior Tcnico, Universidade de Lisboa, Lisbon, Portugal.

Mário Quinta Ferreira: Geosciences Center, Department of Earth Sciences, University of Coimbra, Rua Slvio Lima, 3030-790 Coimbra, Portugal.

Carlos C. Pinto: Halliburton Landmark, 97 Park Dr, Milton, Abingdon OX14 4RY, United Kingdom.

Rui Moura: Instituto de Cincias da Terra (ICT), Faculdade de Cincias da Universidade do Porto, Rua do Campo Alegre, s/n, 4169-007 Porto, Portugal.

José Borges: Institute of Earth Sciences, University of vora, Colgio Luis Antnio Verney, Rua Romo Ramalho, 59, 7002-554 vora Portugal.

Eliza S. Nemser: Seismic Hazards Group, AECOM, 300 Lakeside, Suite 400, Oakland, CA 94612, USA.

Table captions

Table 1: Preliminary set of geologically defined units

Table 2: Results of the Tukey-HSD post-hoc tests

Table 3: Statistics for the final model

Figure captions

Figure 1: a) Tectonic setting of the study area. Seismicity M $\geq$ 3.0, all magnitude scales, according to ISC (2014)(see Data and Resources) is represented for the period 2000-2014; b) Distribution of V_{S30} values in the database. NEHRP site classes (A – $V_{S30} > 1500\,\mathrm{m/s}$; B – $760 < V_{S30} \leq 1500\,\mathrm{m/s}$; C – $360 < V_{S30} \leq 760\,\mathrm{m/s}$; D – $180 < V_{S30} \leq 360\,\mathrm{m/s}$; E - $V_{S30} < 180\,\mathrm{m/s}$) are represented in the background; c) Geographic distribution of V_S depth profiles in the database. The geological units represented are simplified from the 1:500.000 scale geological map of Portugal (Serviços Geológicos de Portugal, 1992); d) Geographic distribution of V_S depth profiles sorted by the characterization method;

Figure 2: V_{S30} as a function of V_{SZ} for $z = 10, 15, 20$, and $25\,\mathrm{m}$. The relationships proposed by Boore (2004) for California are represented by solid lines and their 95% confidence limits by dotted lines. The relationship proposed by Boore *et al.* (2011) for Japan is represented by dashed lines.

Figure 3: Quantiles derived for the normalized V_{S30} and $\log V_{S30}$ data distributions as a function of the theoretical quantiles for the normal distribution. The solid line represents the reference 1:1 line. V_{S30c} and V_{S30z} represent, respectively, the datasets derived using constant extrapolation and extrapolation based on V_{SZ}.

Figure 4: Normalized frequency distribution for $\log V_{S30c}$, sorted by the preliminary set of geologically defined units. The solid line shows the corresponding fitted normal distributions with mean μ and standard deviation σ. The dotted lines correspond to the fitted normal distributions for V_{S30z}. The fitted normal distribution for the declustered P1 dataset ($\mu = 2.9$ and $\sigma = 0.2$) is represented by a dashed line. NEHRP site classes are represented in the background.

Figure 5: Normalized frequency distribution for $\log V_{S30c}$, sorted by the final set of geologically defined units. The solid line shows the corresponding fitted normal distributions with mean μ and standard deviation σ. The dotted lines correspond to the fitted normal distributions for V_{S30z}. NEHRP site classes are represented in the background.

Figure 6: Geographic distribution for the final V_{S30} model; a) log-averaged V_{S30} value, b) upper limit of the 68% confidence interval for the V_{S30} distribution, and c) lower limit of the 68% confidence interval for the V_{S30} distribution.

Figure 7: V_{S30} as a function of slope sorted by the final set of geologically defined units(F1 - Igneous, metamorphic and old sedimentary rocks, F2 - Neogene and Pleistocene formations, F3 - Holocene formations). The boxes outlined in gray represent the V_{S30}-slope class correlations proposed by Wald and Allen (2007) for stable continental regions. The boxes outlined with dashed lines represent tentative V_{S30}-slope class correlations for Holocene data in this study.

Figure 8: Residual distributions of $\log V_{S30}$ with $\log V_{S30}$ values predicted by a) the topographic slope model (see text for details), and b) from the geological analogue method as implemented by Silva *et al.* (2015).

Table 1: Preliminary set of geologically defined units

Name	Geological Unit	General Description
P1	Igneous and metamorphic rocks	Granites, basalts, schists, gabbros, marbles, quartz, turbidites, etc. Includes other formations of Palaeozoic age or older.
P2	Old Sedimentary rocks (Mesozoic or Paleogene age)	Limestones, marly limestones, dolomites, conglomerates and sandstones
P3	Miocene formations	Sands, sandstones, clays and conglomerates
P4	Pliocene formations	Sandstones, gravels, sands and clays
P5	Pleistocene formations	Sand and clays, terrace deposits
P6	Holocene formations	Alluvium, mud, sands, clay, silt and sand dunes

Table 2

Table 2: Results of the Tukey-HSD post-hoc tests

Group pairs	q	p-value	Null hypothesis*
P1-P2	1.308	0.900	accepted
P1-P3	5.827	0.001	rejected
P1-P4	6.480	0.001	rejected
P1-P5	5.114	0.006	rejected
P1-P6	13.164	0.001	rejected
P2-P3	3.902	0.073	accepted
P2-P4	4.562	0.158	accepted
P2-P5	3.428	0.158	accepted
P2-P6	10.481	0.001	rejected
P3-P4	0.939	0.900	accepted
P3-P5	0.201	0.900	accepted
P3-P6	8.331	0.001	rejected
P4-P5	1.030	0.900	accepted
P4-P6	6.984	0.001	rejected
P5-P6	7.449	0.001	rejected
F1-F2	**7.639**	**0.001**	**rejected**
F1-F3	**14.987**	**0.001**	**rejected**
F2-F3	**9.969**	**0.001**	**rejected**

* The null hypothesis is rejected at a 5% significance level.

Table 3: Statistics for the final model

Name	Geological Unit	N	$\mu_{\log V_{S30}}$ *	$\sigma_{\log V_{S30}}$	V_{S30} (m/s)	$V_{S30\ 68\%CI}$ (m/s)†
F1	Igneous, metamorphic and old sedimentary rocks	23	2.91	0.20	829	[523, 1315]
F2	Neogene and Pleistocene formations	55	2.67	0.15	470	[329, 672]
F3	Holocene Formations	29	2.38	0.22	237	[144, 392]

* Represents the log-averaged V_{S30} value

† Represents the 68% confidence interval.

Figure 1a

Click here to download Figure fig_1a.eps

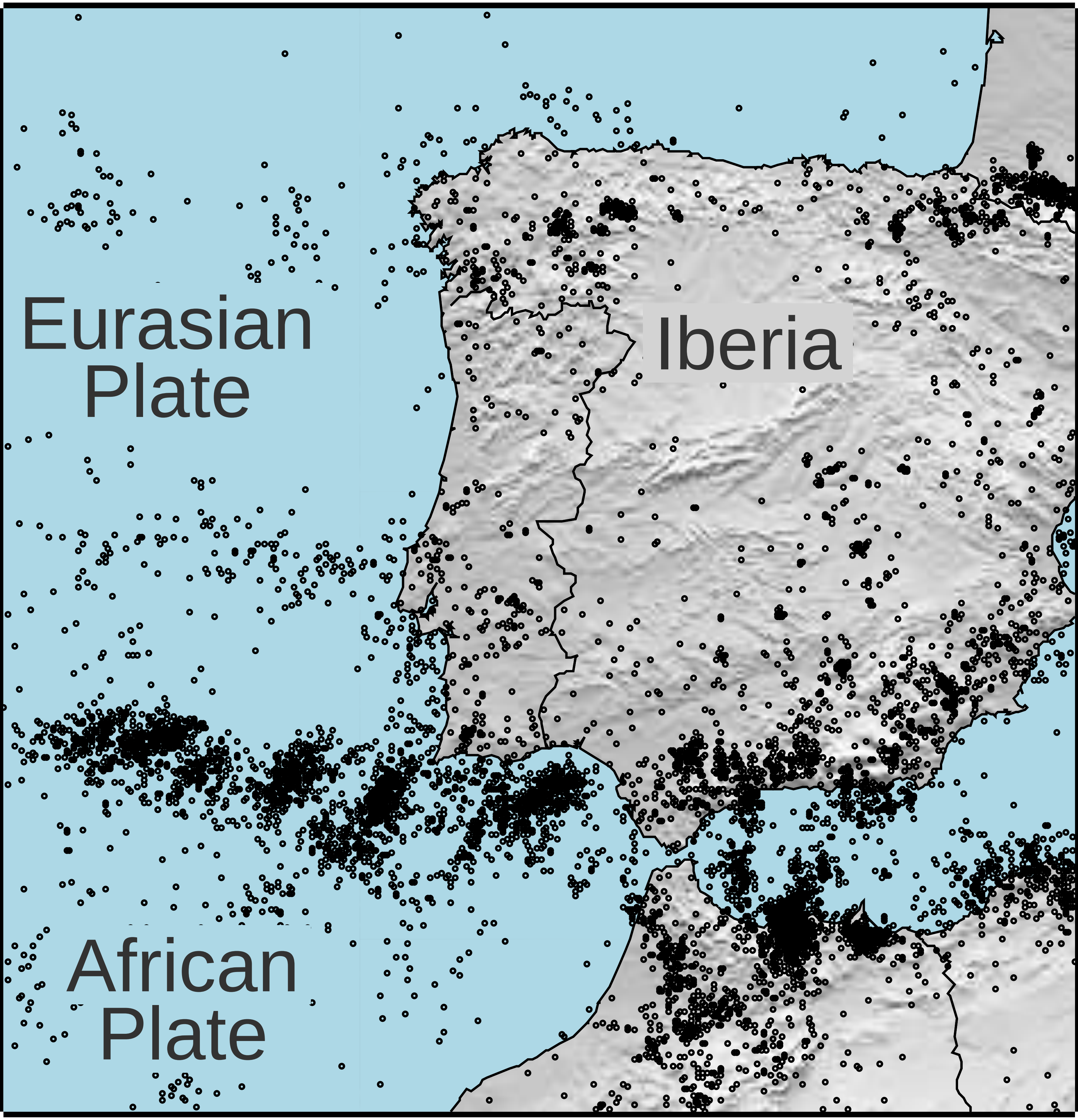

Figure 1b

Click here to download Figure fig_1b.eps

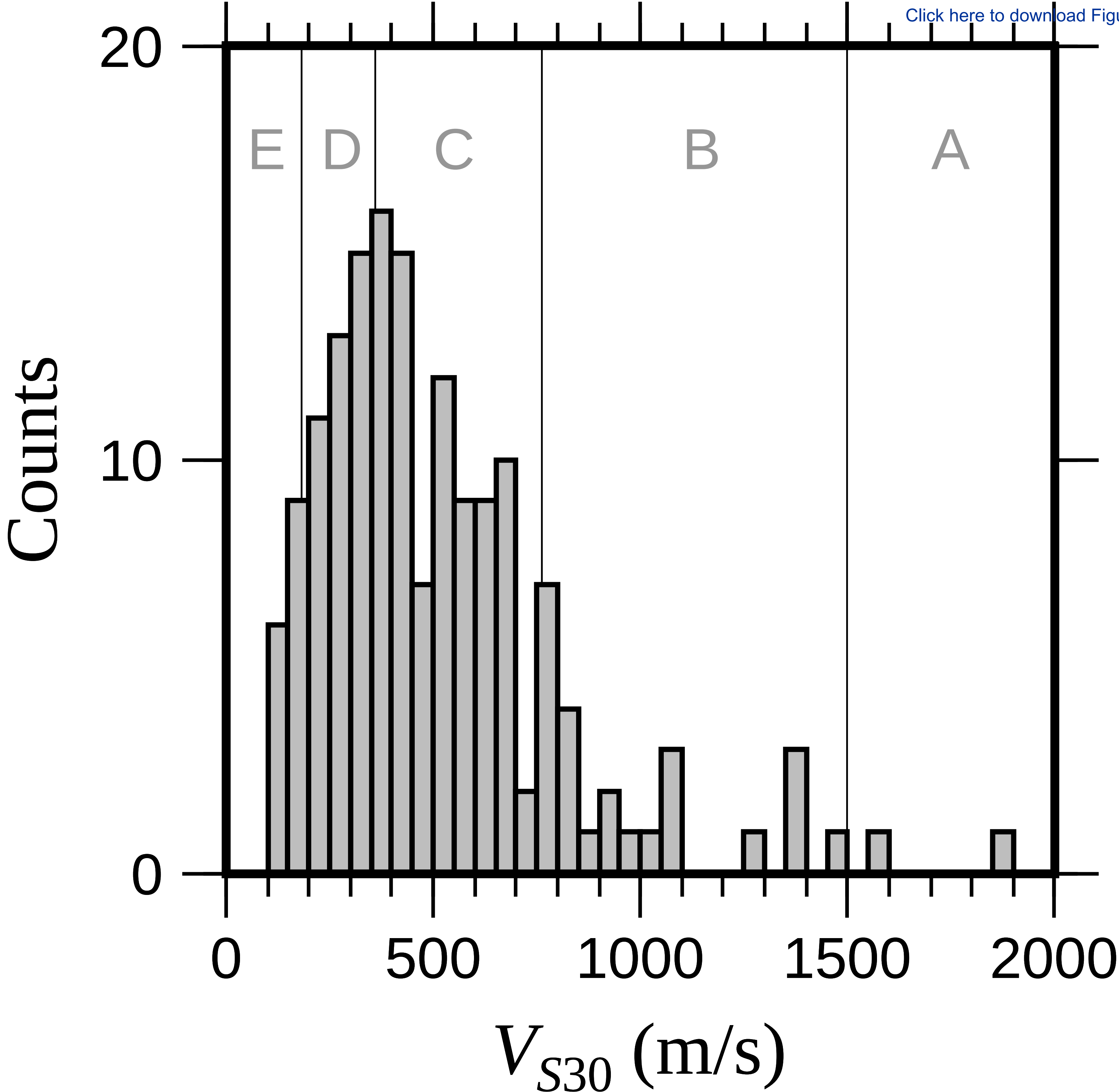

Figure 1c

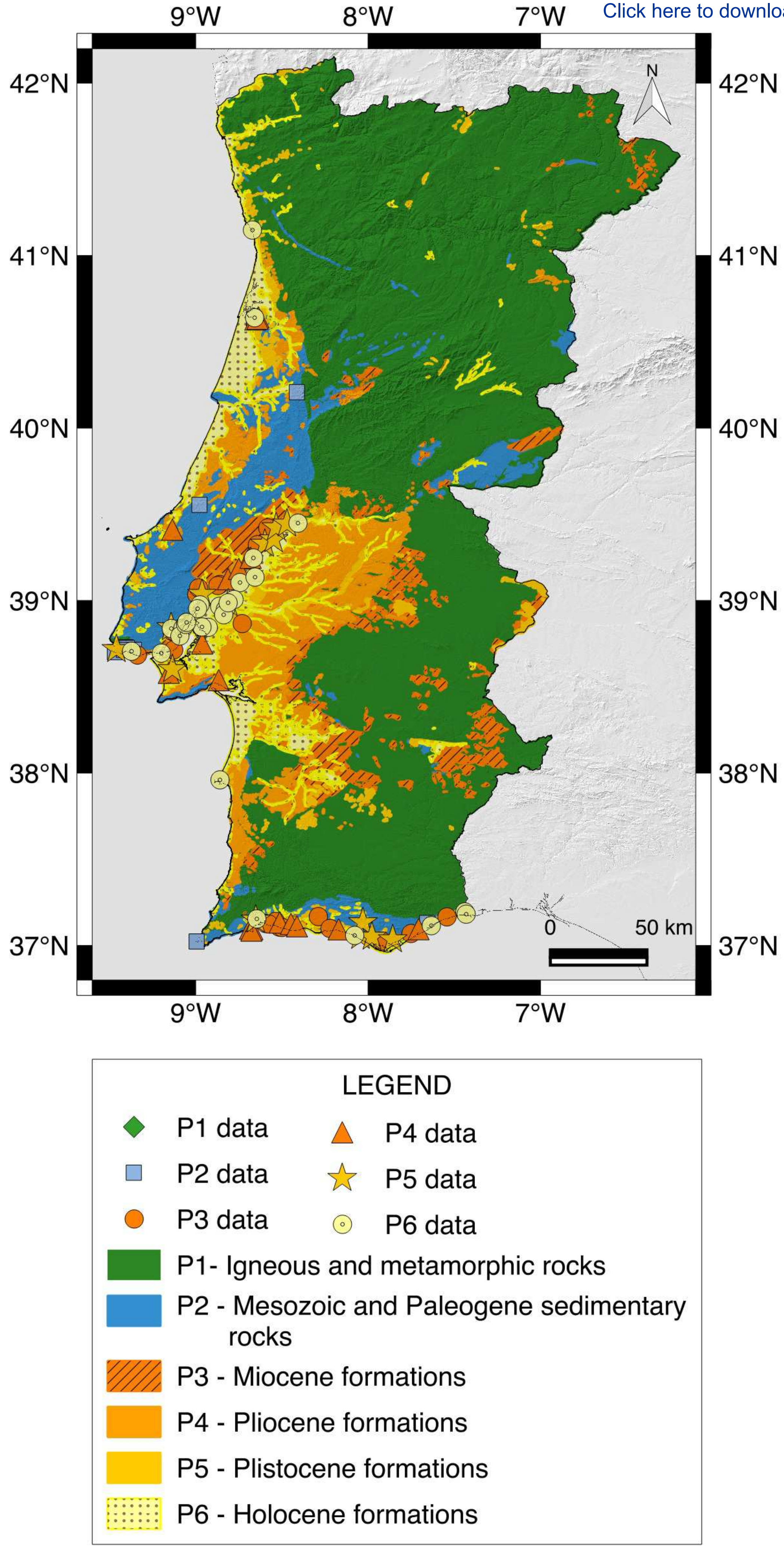
9°W
8°W
7°W
42°N
41°N
40°N
39°N
38°N
37°N
N
0
50 km
LEGEND
P1 data
P2 data
P3 data
P4 data
P5 data
P6 data
P1- Igneous and metamorphic rocks
P2 - Mesozoic and Paleogene sedimentary rocks
P3 - Miocene formations
P4 - Pliocene formations
P5 - Plistocene formations
P6 - Holocene formations

Figure 1d

Click here to download Figure fig_1d.eps

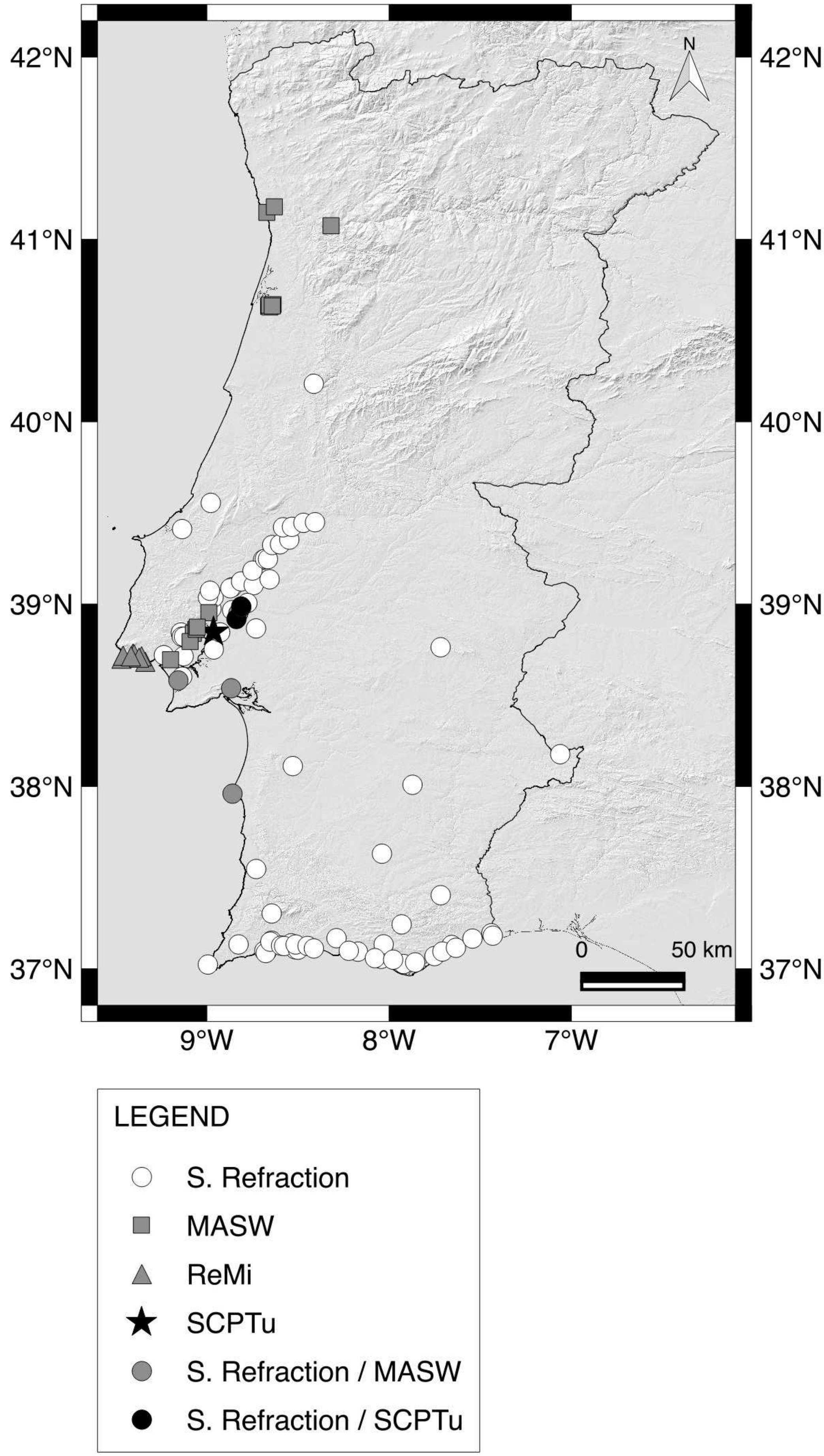

Figure 2

Click here to download Figure fig_2.eps

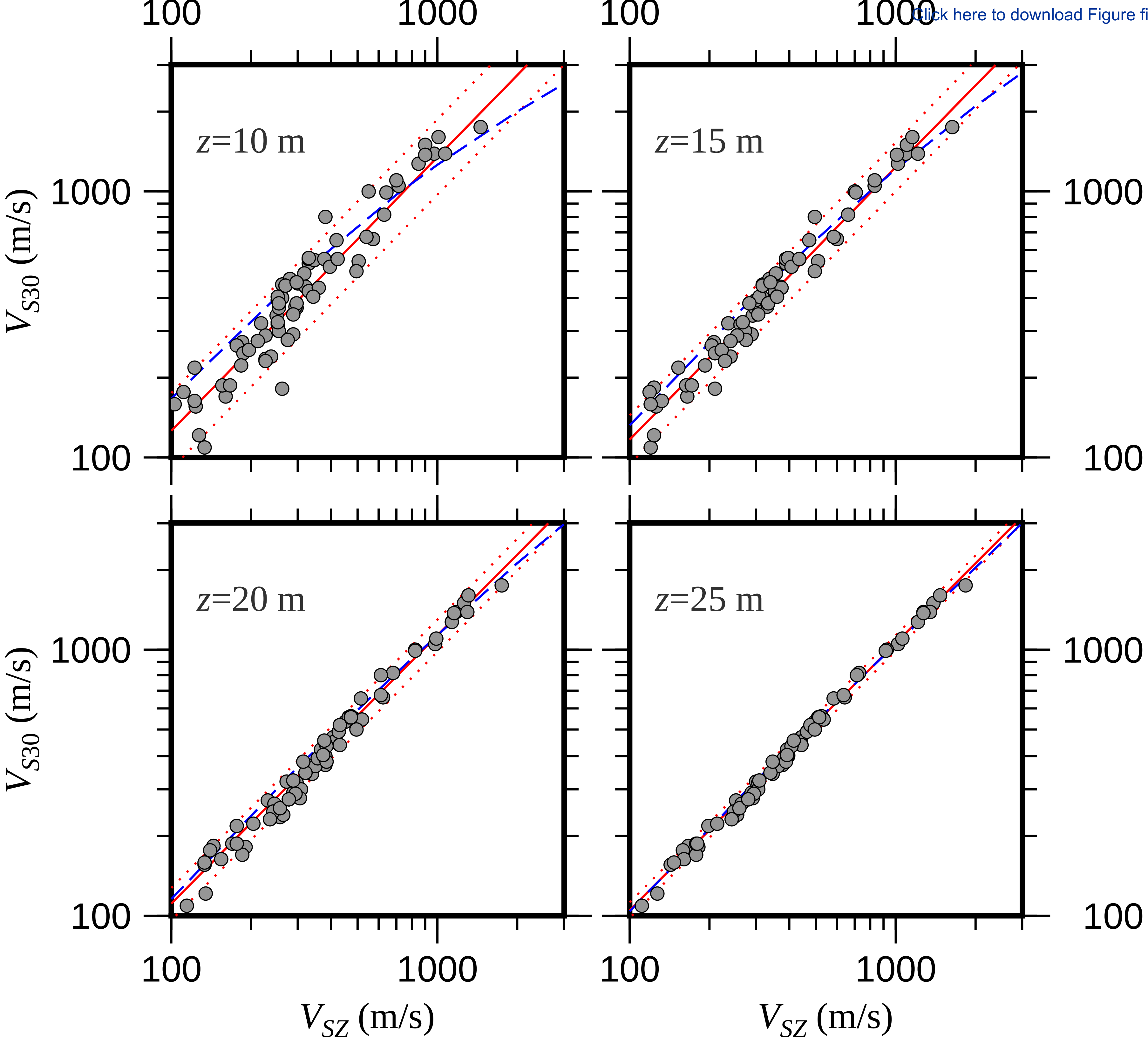

Figure 3

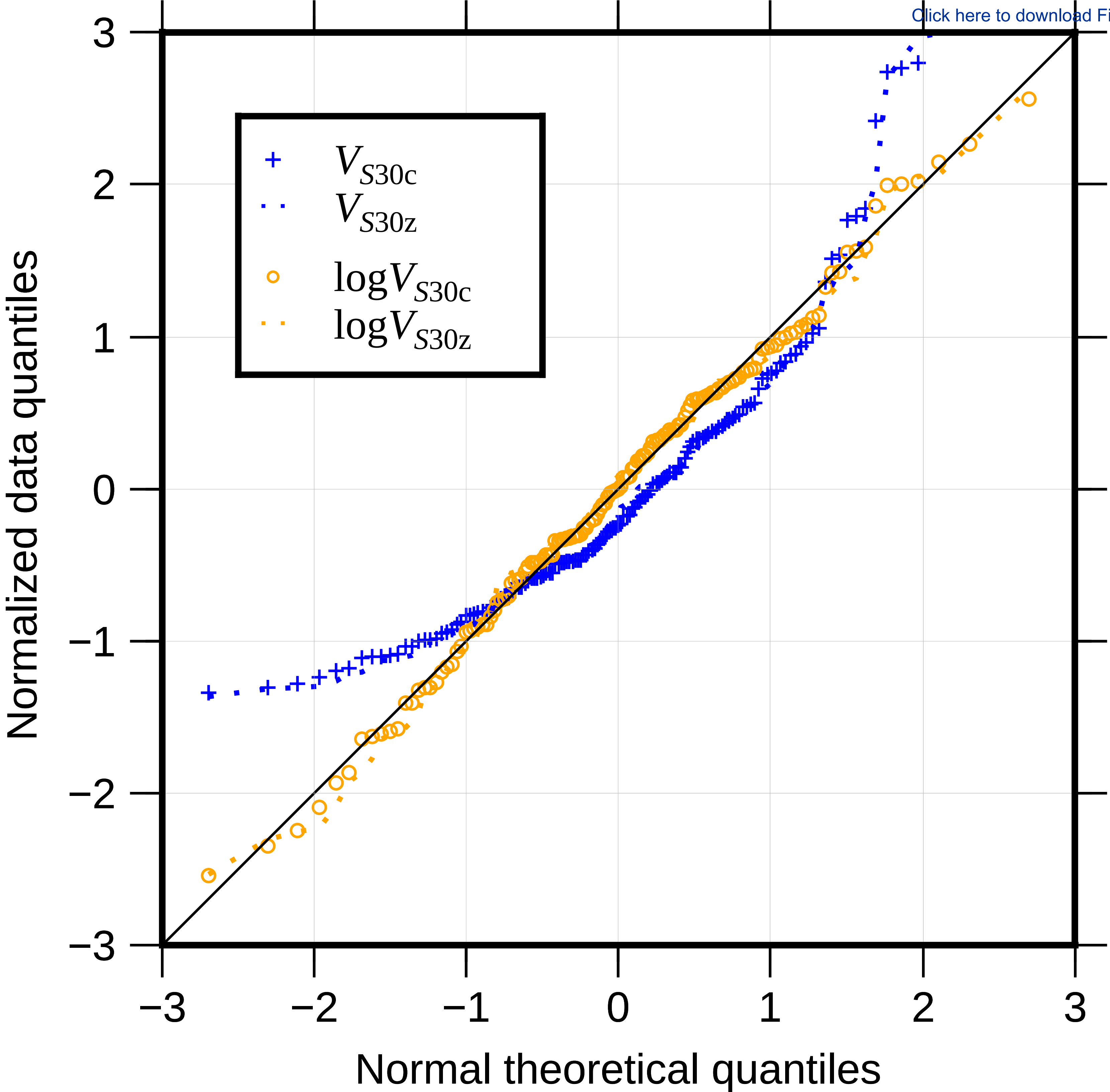
V_{S30c}
V_{S30z}
$\log V_{S30c}$
$\log V_{S30z}$
Normalized data quantiles
Normal theoretical quantiles
3
2
1
0
−1
−2
−3

Figure 4

Click here to download Figure fig_4.eps

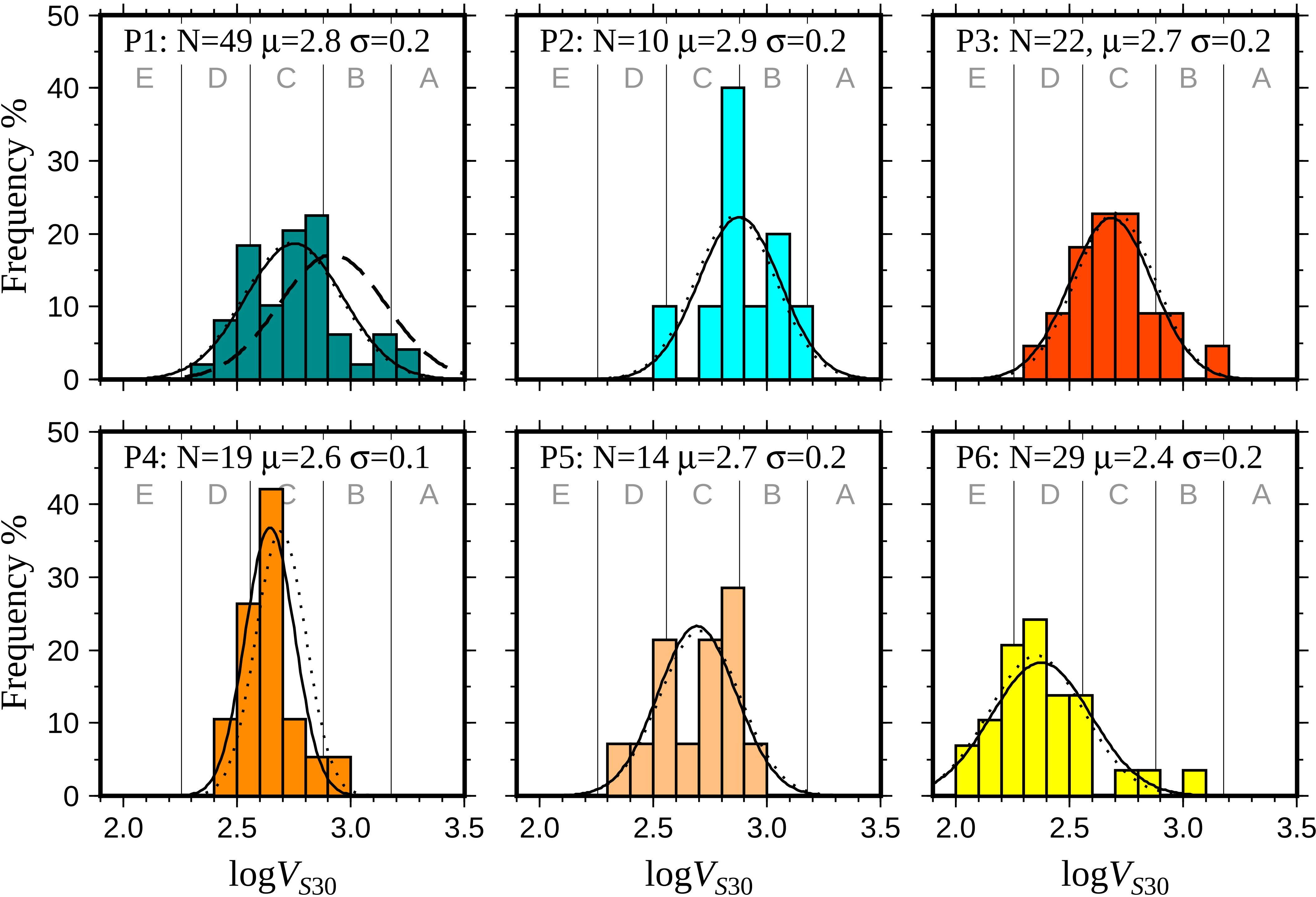

Figure 5

Click here to download Figure fig_5.eps

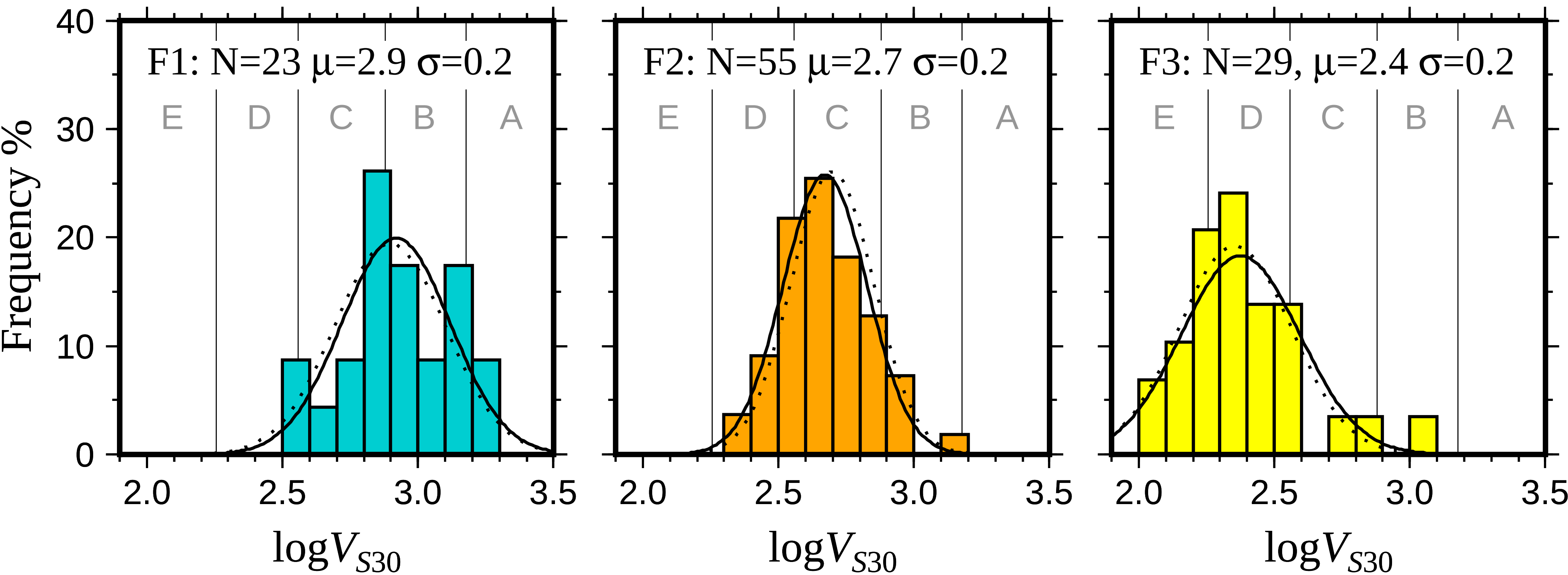

Figure 6a

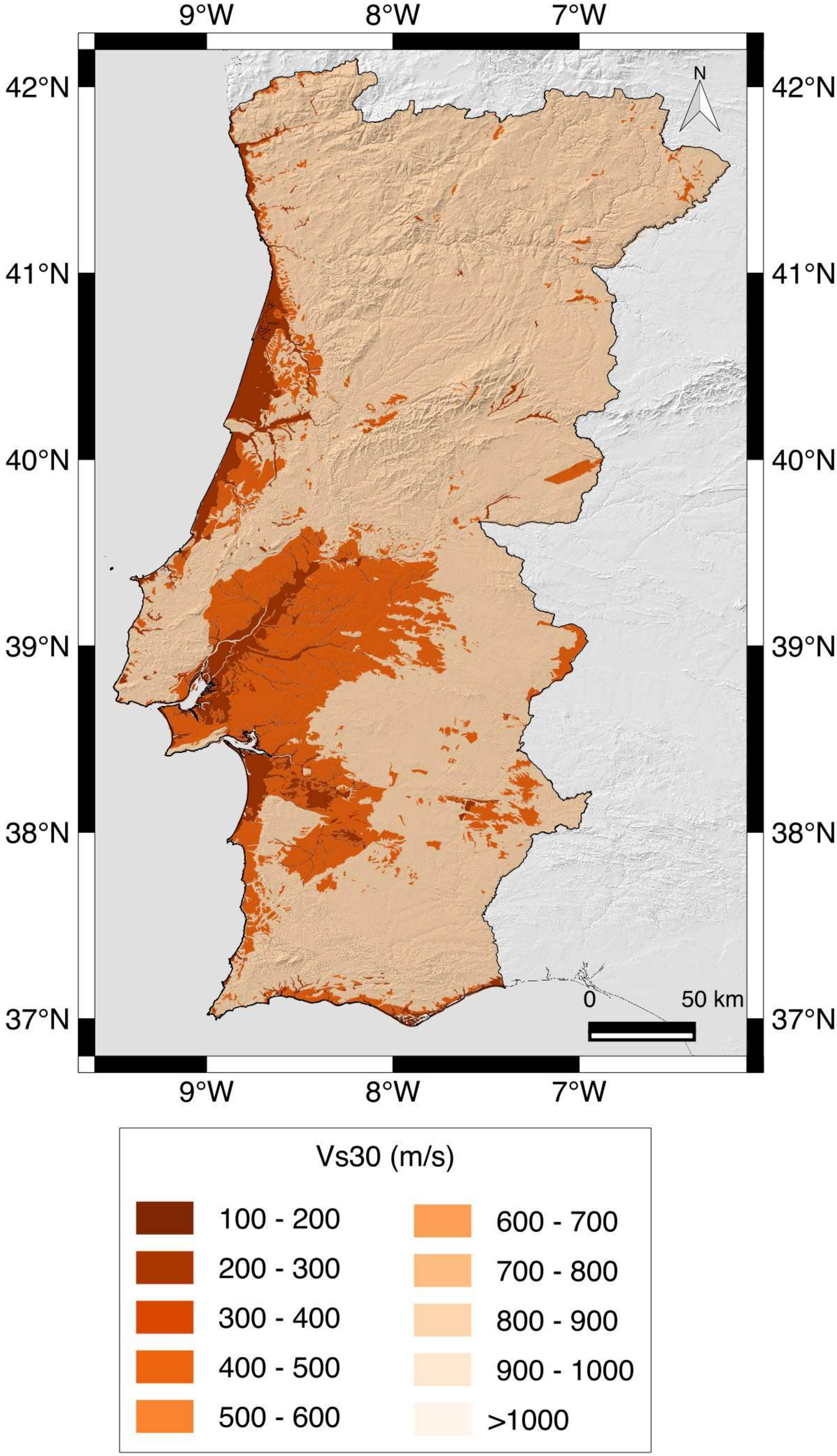
9°W
8°W
7°W
42°N
41°N
40°N
39°N
38°N
37°N
N
0
50 km
Vs30 (m/s)
100 - 200
200 - 300
300 - 400
400 - 500
500 - 600
600 - 700
700 - 800
800 - 900
900 - 1000
>1000

Figure 6b

Click here to download Figure fig_6b.eps

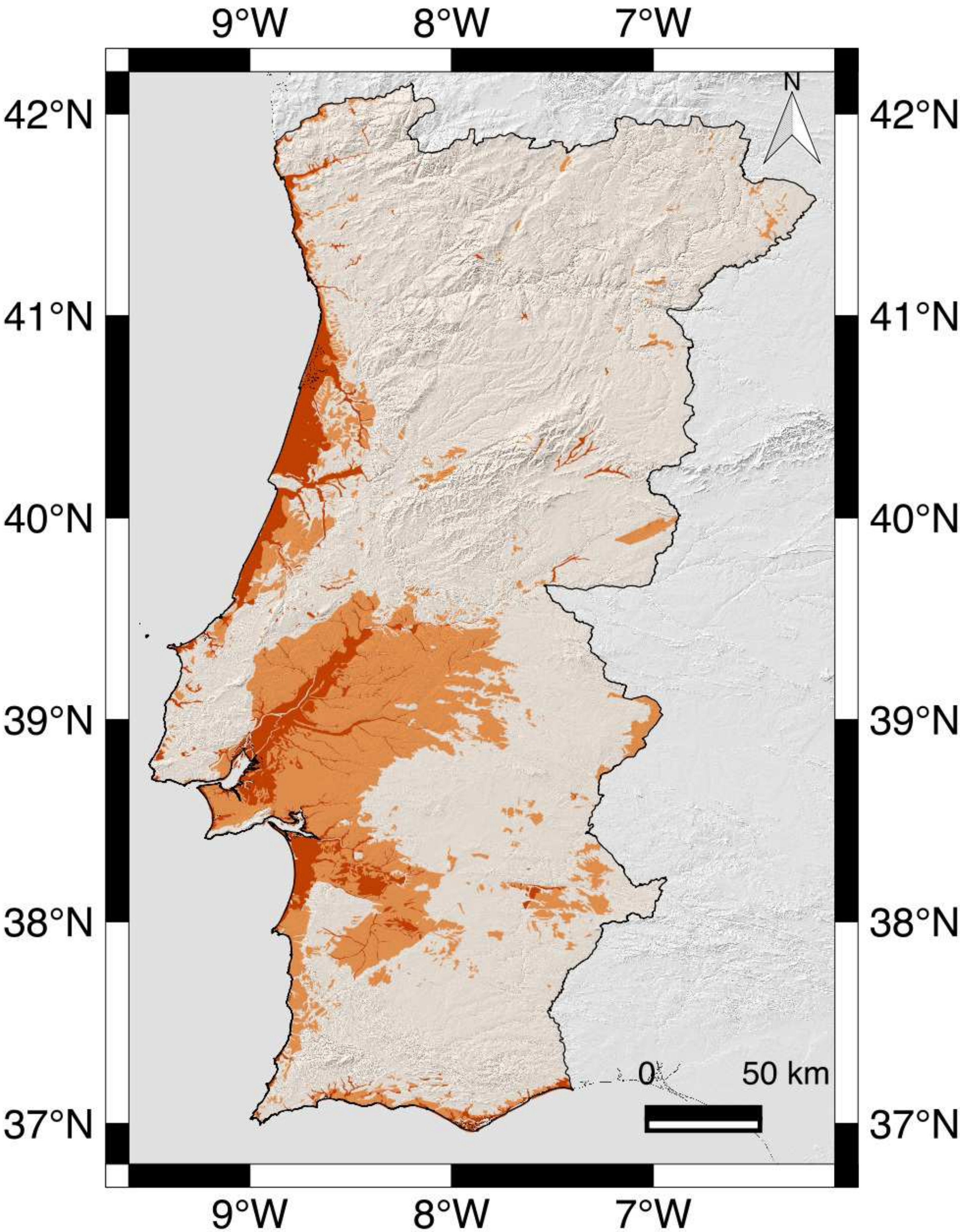

Figure 6c

Click here to download Figure fig_6c.eps

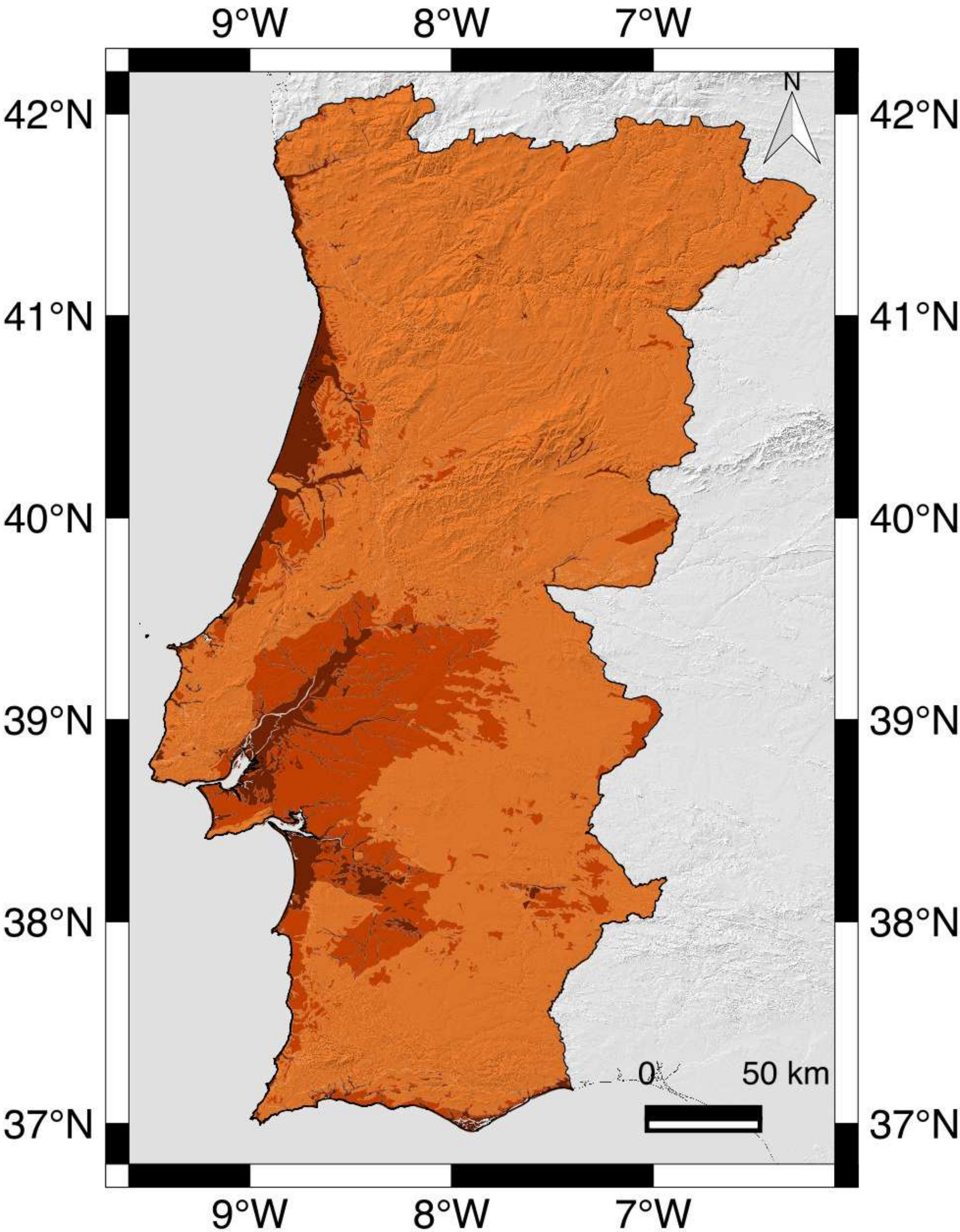

Figure 7

Click here to download Figure fig_7.eps

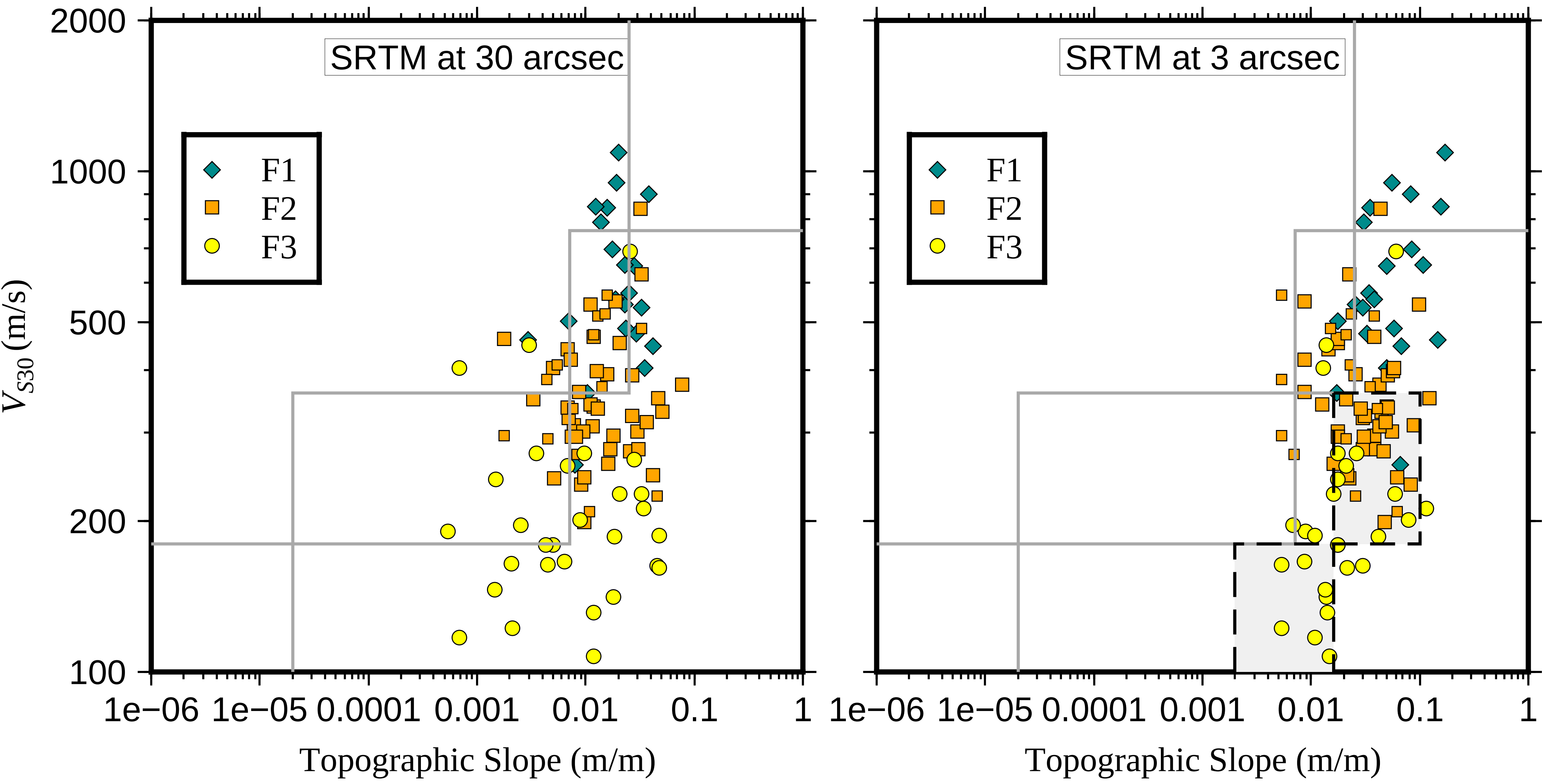

Figure 8a

Click here to download Figure fig_8a.eps

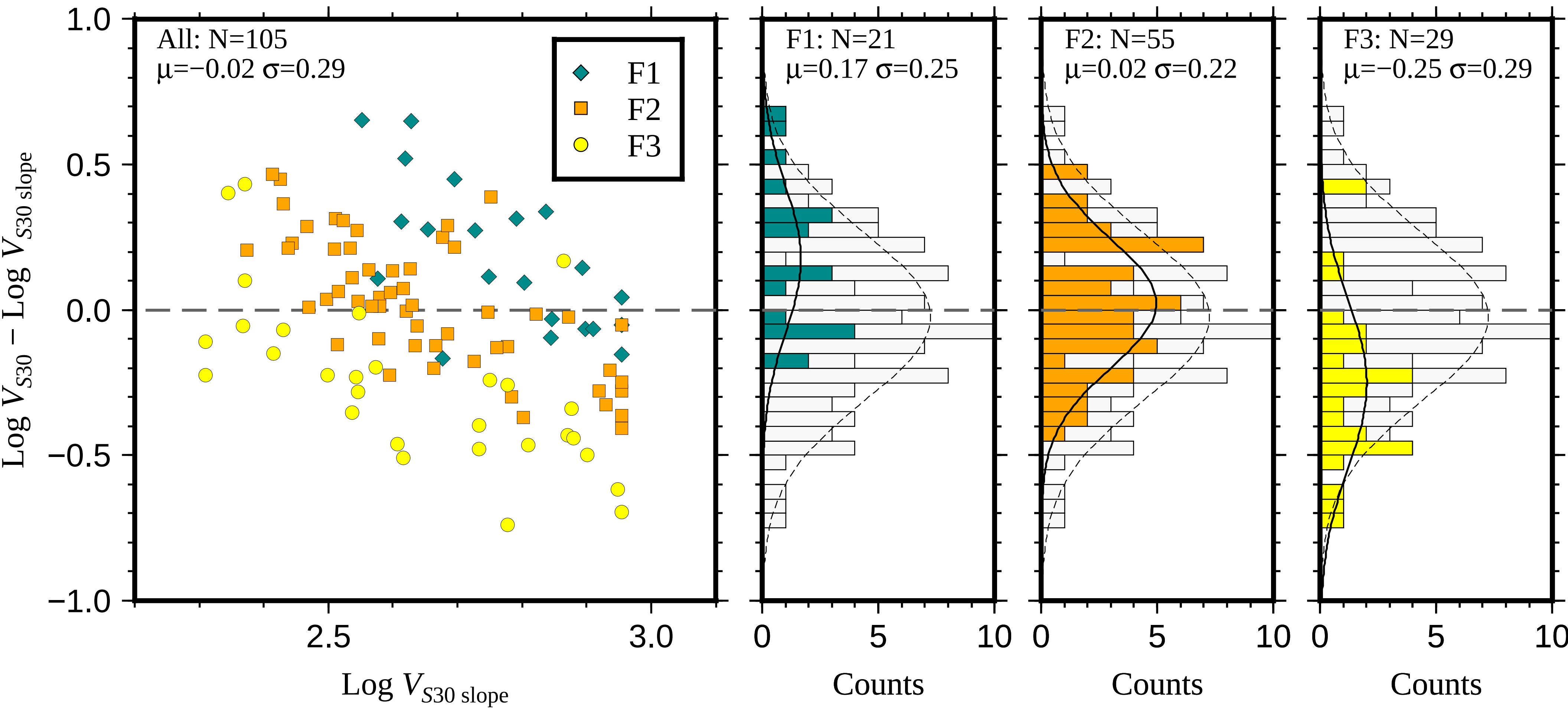

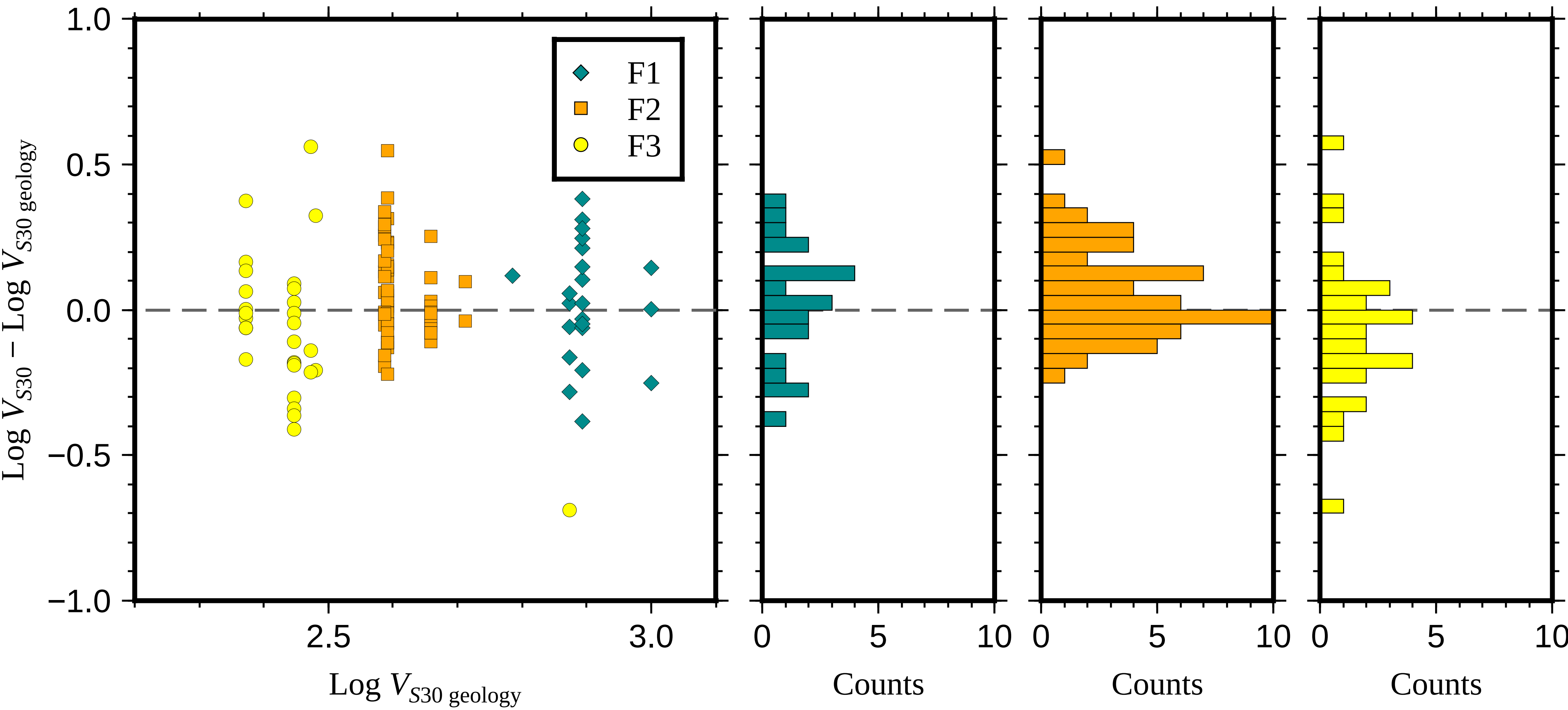

1.0
0.5
0.0
−0.5
−1.0
Log V_{S30} − Log $V_{S30\ \mathrm{geology}}$
2.5
3.0
Log $V_{S30\ \mathrm{geology}}$
F1
F2
F3
0
5
10
Counts
0
5
10
Counts
0
5
10
Counts

Figure 1 composed example Click here to download Figure fig_1_composed_example.png

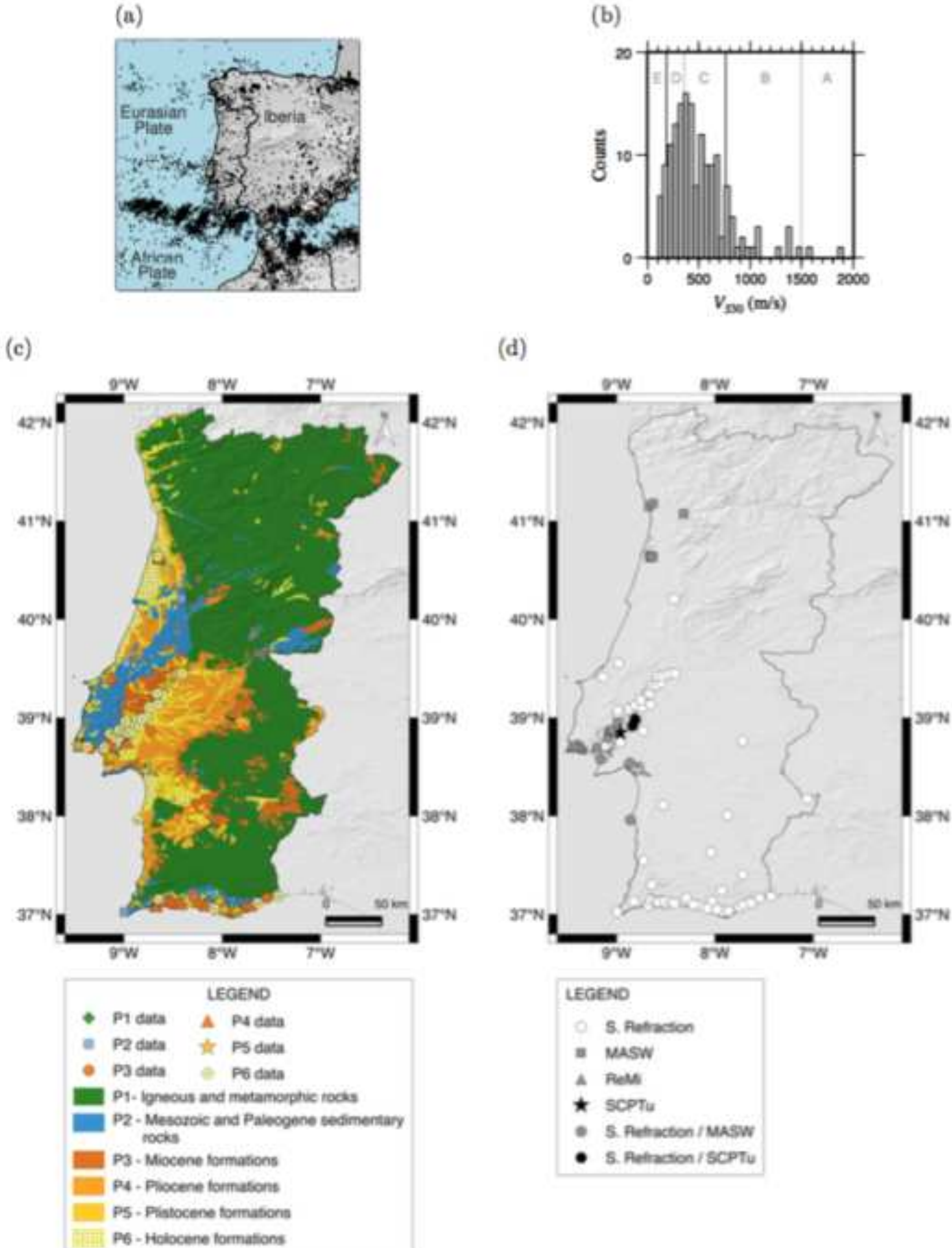

Figure 6 composed example

Click here to download Figure fig_6_composed_example.eps

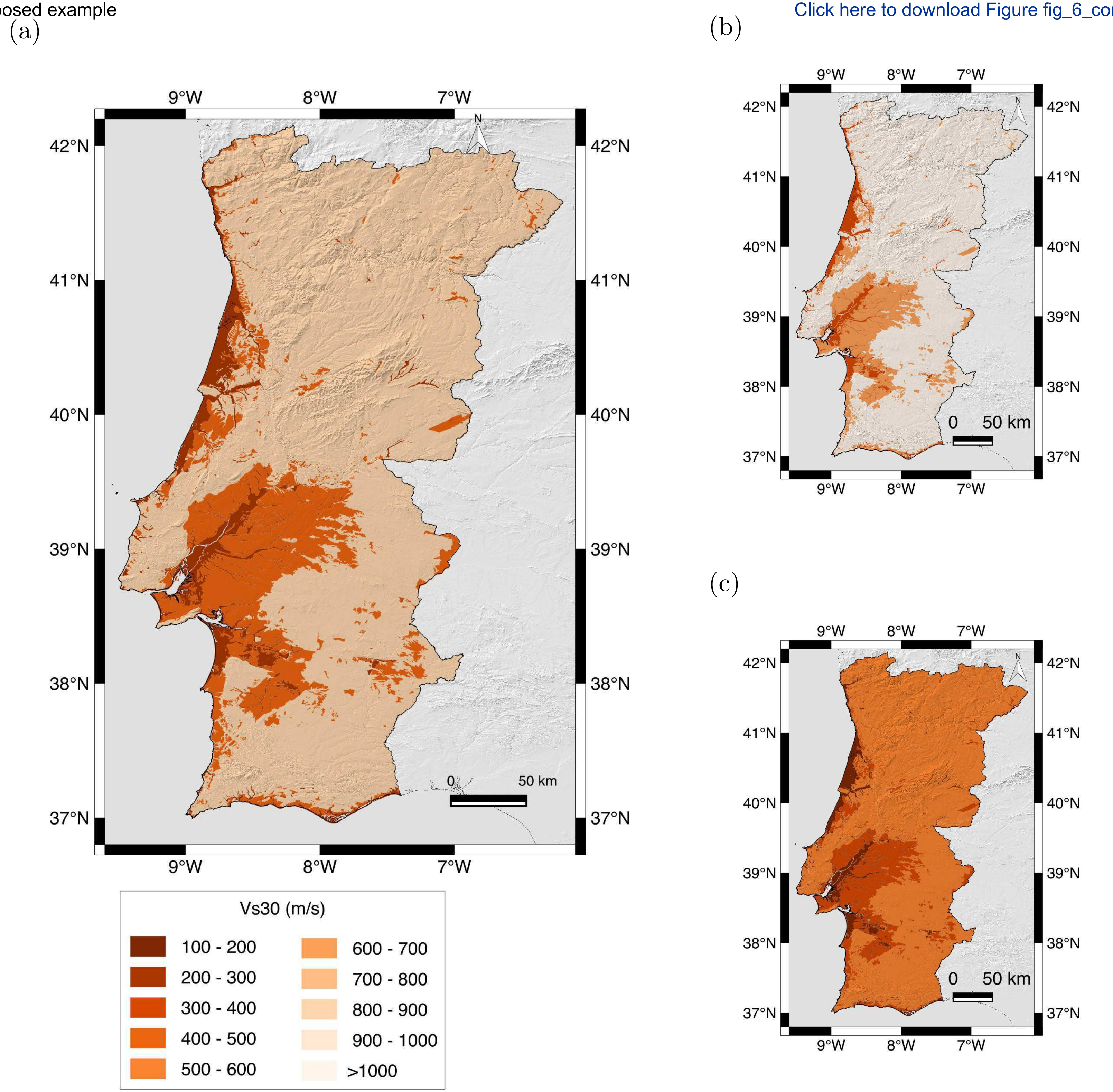

Figure 8 composed example

Click here to download Figure fig_8_composed_example.eps

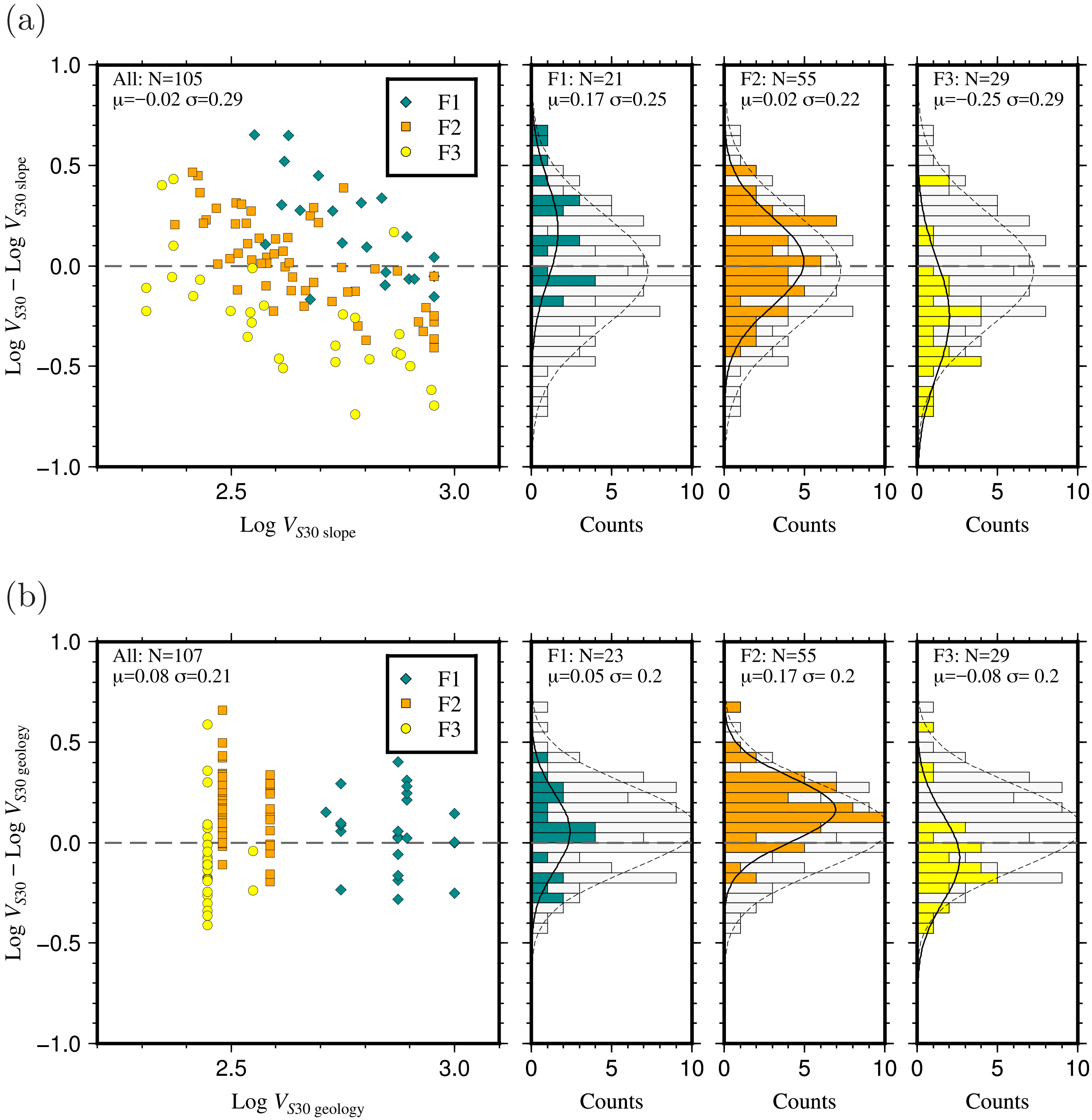

Electronic Supplement to

Developing a Geologically-Based V_{S30} Site-Conditions Model for Portugal: Methodology and Assessment of the Performance of Proxies

by

Susana P. Vilanova, João Narciso, João P. Carvalho, Isabel Lopes, Mário Quinta-Ferreira, Carlos C. Pinto, Rui Moura, José Borges, and Eliza S. Nemser

This electronic supplement includes a spreadsheet file containing the database used in this paper (Table S1).

Table S1 – Plain text comma separated values (csv) file including location of the profiles, methodology used to estimate the V_S depth structure, elevation and topographic slope calculated using both the SRTM30 and the SRTM30 datasets, geological classification using maps at 1:500.000, 1:200:000 and 1:50:000 scales, depth value z for which V_S information is available, V_{SZ} calculated, V_{S30} calculated from correlations with V_{SZ}, V_{S30} calculated using constant extrapolation, variability of $\log V_{S30}$, and V_{S30} calculated from topographic slope, and associated notes and remarks.

Bulletin of the Seismological Society of America

COPYRIGHT/PUBLICATION-CHARGES FORM

PLEASE FILL OUT AND SUBMIT THIS FORM ONLINE WHEN SUBMITTING YOUR PAPER

Manuscript Number: BSSA-D- ______________________[leave blank for new submissions]

Title: Developing a Geologically-Based VS30 Site-Conditions Model for Portugal: Methodology and Assessment of the Performance of Proxies

Authors: Susana P. Vilanova, João Narciso, João P. Carvalho, Isabel Lopes, Mário Quinta-Ferreira, Carlos C. Pinto, Rui Moura, José Borges, Eliza S.Nemser

COPYRIGHT

20/07/ 2017

Authorized Signature for Copyright | Print Name (and title, if not author) | Date

PUBLICATION CHARGES

The Seismological Society of America requests that institutions supporting research share in the cost of publicizing the results of that research. The Editor has the discretion of waiving publication charges for authors who do not have institutional support. If pages are paid for by SSA, then no further page charge waivers can be requested for two years by any author listed on the paper. Page charges for waived papers cannot exceed 12 printed pages. Rejected papers in which a page waiver was requested will be considered toward the limit of one request per two years. In addition to regular publication charges there is a nominal fee for publishing electronic supplements, which will not be waived. Current rates are available at http://www.seismosoc.org/publications/journal-publication-charges/.

Color options: Color figures can be published (1) in color both in the online journal and in the printed journal, or (2) in color online and gray scale in print. Online color is free; authors will be charged for color in print. You must choose one option for all of the color figures within a paper; that is, you cannot choose option (1) for one color figure and option (2) for another color figure. You cannot submit two versions of the same figure, one for color and one for gray scale. You are responsible for ensuring that color figures are understandable when converted to gray scale, and that text references and captions are appropriate for both online and print versions. Color figures must be submitted before the paper is accepted for publication.

Art guidelines are at http://www.seismosoc.org/publications/bssa/bssa-art-submission-guidelines/

Will publication charges be paid? Check one:

_____ **BOTH PUBLICATION CHARGES AND COLOR CHARGES WILL BE PAID**, and all color figures for this paper will be color both online and in print. This option requires full payment of publication & color charges.

_x_ **ONLY PUBLICATION CHARGES WILL BE PAID**, and all figures for this paper will be gray scale in print. Color figures, if any, will be color online.

_____**REQUEST A REDUCTION IN PUBLICATION CHARGES.** Send a letter of request and explanation to the Editor-in-Chief at BSSAeditor@seismosoc.org. Color figures, if any, will be color online but gray scale in print.

Send Invoice to: IST-ID, VAT: 509 830 072; Address: IST, CERENA Av. Rovisco Pais, 1, 1049-003 Lisboa

If your paper is accepted for publication, SSA requires that you fill out and submit your final files.

Questions regarding billing should be directed to the SSA Business Office,
400 Evelyn Avenue, Suite 201 Albany, CA 94706 USA Phone 510 525-5474 Fax 510 525-7204